Geological Quarterly, 2025, 69, 16
DOI: https://doi.org/10.7306/gq.1789

Fusing GRACE data into terrestrial water budgets to improve their predictive performance: a case study of the Bug River Transboundary Catchment, Polish-Ukrainian-Belarusian borderland

Tatiana SOLOVEY[1, *], Justyna ŚLIWIŃSKA-BRONOWICZ[2], Rafał JANICA[1], Agnieszka BRZEZIŃSKA[1] and Anna STRADCZUK[3]

[1] Polish Geological Institute – National Research Institute, Rakowiecka 4, 00-975 Warszawa, Poland; ORCID: 0000-0001-8949-4075 [T.S.], 0009-0001-7142-5570 [R.J.], 0009-0006-2007-9053 [A.B.]

[2] Centrum Badań Kosmicznych Polskiej Akademii Nauk (CBK PAN), Bartycka 18a, 00-716 Warszawa, Poland; ORCID: 0000-0001-7502-5243

[3] University of Warsaw, Faculty of Geology, Żwirki i Wigury 93, 02-089 Warszawa, Poland; ORCID: 0009-0007-6307-0101

Solovey, T., Śliwińska-Bronowicz, J., Janica, R., Brzezińska, A., Stradczuk, A., 2025. Fusing GRACE data into terrestrial water budgets to improve their predictive performance: a case study of the Bug River Transboundary Catchment, Polish-Ukrainian-Belarusian borderland. Geological Quarterly, 69, 16; https://doi.org/10.7306/gq.1789

Associate Editor: Beata Jaworska-Szulc

We analysed variations in terrestrial water storage (TWS) over the Bug River Transboundary Catchment for the period 2012–2023. To do so, we utilized satellite gravimetry data from the Gravity Recovery and Climate Experiment (GRACE) mission, along with satellite and *in situ* components of the water balance (WB) approach, including precipitation, evapotranspiration, and runoff. TWS anomalies and month-to-month changes in TWS (TWS) derived from GRACE data (TWS-GRACE/ TWS-GRACE) were compared with those from the water balance approach (TWS-WB/ TWS-WB) for the study area. The results showed a good agreement between TWS-GRACE and TWS-WB, with an average coefficient of determination of 0.77. This agreement is slightly stronger in the lowland areas and weaker in the upland regions. We also found that this consistency decreases during the dry months (April to September). In the next step, we performed data assimilation of GRACE and hydrometeorological data by applying a regression-based model. Our results demonstrated that such data fusion effectively mitigates the uncertainties in TWS-GRACE related to its low spatial and temporal resolution, improving the consistency between TWS-GRACE and TWS-WB, as shown by a reduction in root mean square error from 34.7 to 14.9 mm/month. The results revealed that between 2012 and 2023 the Bug River Basin faced alternating extreme decreases and increases in TWS. Although the magnitude of the trends varied slightly over different periods, the overall region exhibited negative trends in TWS changes, with an average rate of ~9 mm/year.

Key words: GRACE, terrestrial water storage, water budget, Bug River.

INTRODUCTION

The Gravity Recovery and Climate Experiment (GRACE) satellite mission and its successor GRACE Follow-On (GRACE-FO; the GRACE and GRACE-FO missions will be collectively referred to as "GRACE" hereafter) provided an unprecedented opportunity to track the global dynamics of cumulative changes in terrestrial water storage (TWS) at a previously unattainable level. This marked a breakthrough in monitoring the continental phase of the water cycle (Tapley et al., 2019). TWS from GRACE effectively closes the water balance, which represents the equilibrium between precipitation (P), water losses through evapotranspiration (ET), streamflow (R), and changes in TWS (TWS). TWS is crucial for understanding the effects of climate change and is recognized by the Global Climate Observing System (GCOS) as one of the essential climate variables.

An important aspect of regional TWS studies is the sensitivity of GRACE measurements to changes in water mass and the associated spatial resolution. The effective spatial resolution of GRACE satellite data for hydrology and hydrogeology remains a topic of ongoing discussion (Frappart et al., 2018; Vishwakarma et al., 2018). It depends on the size of the area, but is also influenced by its physical-geographical characteristics, the size of water resources in the region, and the magnitude of their variability. The spatial resolution of GRACE measurements is generally estimated to be ~300 × 300 km (Tapley et al., 2004; Wahr et al., 2004, 2006). The GRACE measure-

* Corresponding author, e-mail: tatiana.solovey@pgi.gov.pl

Received: April 2, 2025; accepted: May 12, 2025; first published online: July 21, 2025

ment sensitivity allows detection of water-height changes of ~1–2 cm over spatial scales of 300 km, which represents the smallest native scale at which GRACE can resolve a mass change signal. However, Lorenz et al. (2014) confirmed the high detectability of TWS changes at smaller spatial scales (<100,000 km^2), if the observed variations have a strong seasonal cycle. A study by Vishwakarma et al. (2018) showed that GRACE can capture TWS changes over areas of ~63,000 km^2, while Tourian et al. (2018) indicated that such changes can be observed even in areas of 52,000 km^2.

At present, GRACE remains the only source of direct information about TWS. However, the low spatial resolution of GRACE products and periodic degradation in signal quality limit their utility for monitoring the water cycle at regional scale (Vishwakarma et al. 2018). Therefore, many recent studies utilizing GRACE data for monitoring water resources address the challenging topic of increasing the spatial resolution of GRACE data (Rowlands et al., 2005; Miro and Famiglietti, 2018; Sun et al., 2019; Vishwakarma et al., 2021; Zhong et al., 2021; Pascal et al., 2022; Yin et al., 2022) or improving the measurements' precision (Becker et al., 2011; Frappart et al., 2013; van Dijk et al., 2014; Long et al., 2015; Chen et al., 2022).

In this study, we focused on improving TWS estimates by combining observations of water balance (WB) components and TWS derived from the GRACE mission. In the context of the water balance, TWS change can be defined as $TWS = P - ET - R$, assuming 100% closure of the balance. Despite efforts to achieve high-resolution global monitoring of the terrestrial water cycle, significant challenges remain in providing physically consistent and accurate estimates of water balance components. These challenges include the uncertainty in estimating individual components derived from different satellite sensors and models, and the low spatial and temporal resolution of available data (Sahoo et al., 2011). The primary reason for the inability to perfectly close the water balance is that no single satellite sensor measures all water balance components simultaneously. Nevertheless, considering the availability of in-situ measurements, there is potential to combine individual component estimates into a physically consistent, comprehensive estimate of the water cycle balance.

A comparison of TWS estimates derived from the water balance approach and GRACE data generally indicates good agreement between these two methods. Research conducted on the ten largest river basins in the world (Sahoo et al., 2011), for China (Long et al., 2015), and Africa (Hassan and Jin, 2016; Nanteza et al., 2016) showed that the coefficient of determination (R_c) between TWS variations from those two approaches reaches values of 0.6–0.8.

This study focuses on assessing and comparing the accuracy of TWS estimates from GRACE with water balance data in the transboundary Bug River Basin, located at the Polish-Ukrainian-Belarusian border, using statistical methods. Regression models were developed to relate TWS to various predictor variables. This approach allowed for the identification of spatio-temporal patterns in the discrepancies between TWS estimated using water balance method and those observed by GRACE.

In Poland, the Bug River Basin is considered one of the most affected by reduced water resources due to climate warming, with river discharge estimated to have decreased by ~20% compared to the 1951–1988 period (Urban et al., 2022; Kostrzewski and Abramowicz, 2023). However, although there is a substantial amount of research on water security, quality and flow in the Bug River Basin (e.g., Gopchak et al., 2020; Shakhman and Bystriantseva, 2020; Grzywna et al., 2021; Snizhko et al., 2024a, b), there are no studies that would focus on the quantitative analysis of TWS resources in the region. Hence, analysis of TWS changes based on GRACE observations and water balance estimates has great potential for monitoring water resources in this region. It can also contribute to improving integrated water resource management at the catchment scale.

The specific objectives of this study were as follows: (1) determining scaling factors for the Bug River Basin to reconcile TWS-GRACE with modelled TWS from the water balance approach (TWS-WB); (2) assessing differences in TWS estimation using the water balance approach and GRACE data; (3) conducting a water cycle reanalysis for the period 2012–2023 by merging satellite gravimetry, satellite-derived precipitation (P) and evapotranspiration (ET) products, and in-situ streamflow data.

By achieving these objectives, we highlight the usefulness of the water balance equation for filling gaps in TWS-GRACE time series and correcting low-quality measurement data. Moreover, our assessment helps to understand the potential of water balance computations for downscaling TWS-GRACE in the Bug River Basin. This multi-source dataset of the main water balance components provides an opportunity to enhance the resolution of TWS-GRACE.

STUDY AREA

The study area encompasses the Bug River Basin (38,712 km^2), located at the intersection of Poland, Ukraine, and Belarus (Fig. 1). With a length of 772 km, it is a major transboundary waterway in Eastern Europe with a catchment area of ~40,000 km^2. The basin features a complex structure, situated within two distinct physical-geographical regions: the East Baltic-Belarusian Lowlands and the Ukrainian Highlands (Kondracki, 2011). Most of the area (75%) comprises lowlands with elevations between 100–200 metres above sea level (m a.s.l.), while the highlands (25%) reach a maximum of 400 m a.s.l (Fig. 1). Based on geomorphological divisions, the Bug River Basin is divided into the upper part within the highlands and the lower part in the lowlands. The Bug River is characterized by a complex, snow-rainfall regime with a clear dominance of winter runoff and groundwater contributions ranging from 40 to 60% (Wrzesiński and Sobkowiak, 2018).

The climate in the catchment area is temperate humid. It evolved at the intersection of two climatic regions: the dry continental and the humid mountain climates. The average annual air temperature is 7.3°C, with the lowest temperatures occurring in January (–4°C) and the highest in July (18–19°C; Lorenc, 2005). The average annual precipitation is around 562 mm, dropping below 400 mm in dry years and exceeding 850 mm in wet years (Fig. 1). The months with the highest precipitation are June and July, with an average of 75–80 mm of rainfall, while February and March have the lowest precipitation, with an average monthly rainfall of 30 mm. The average annual precipitation slightly exceeds evapotranspiration (Fig. 1), which amounts to 490 mm (Szwed, 2015).

DATA USED

GRACE DATA

For TWS anomalies determined from GRACE measurements, we use a mascon solution provided by the Center for Space Research (CSR) – CSR RL06.3 (Save et al., 2016; Save, 2020). In the mascon approach, the area of Earth is divided into predefined areas called "mascons" (mass concentrations). Each mascon aggregates changes in gravity over that

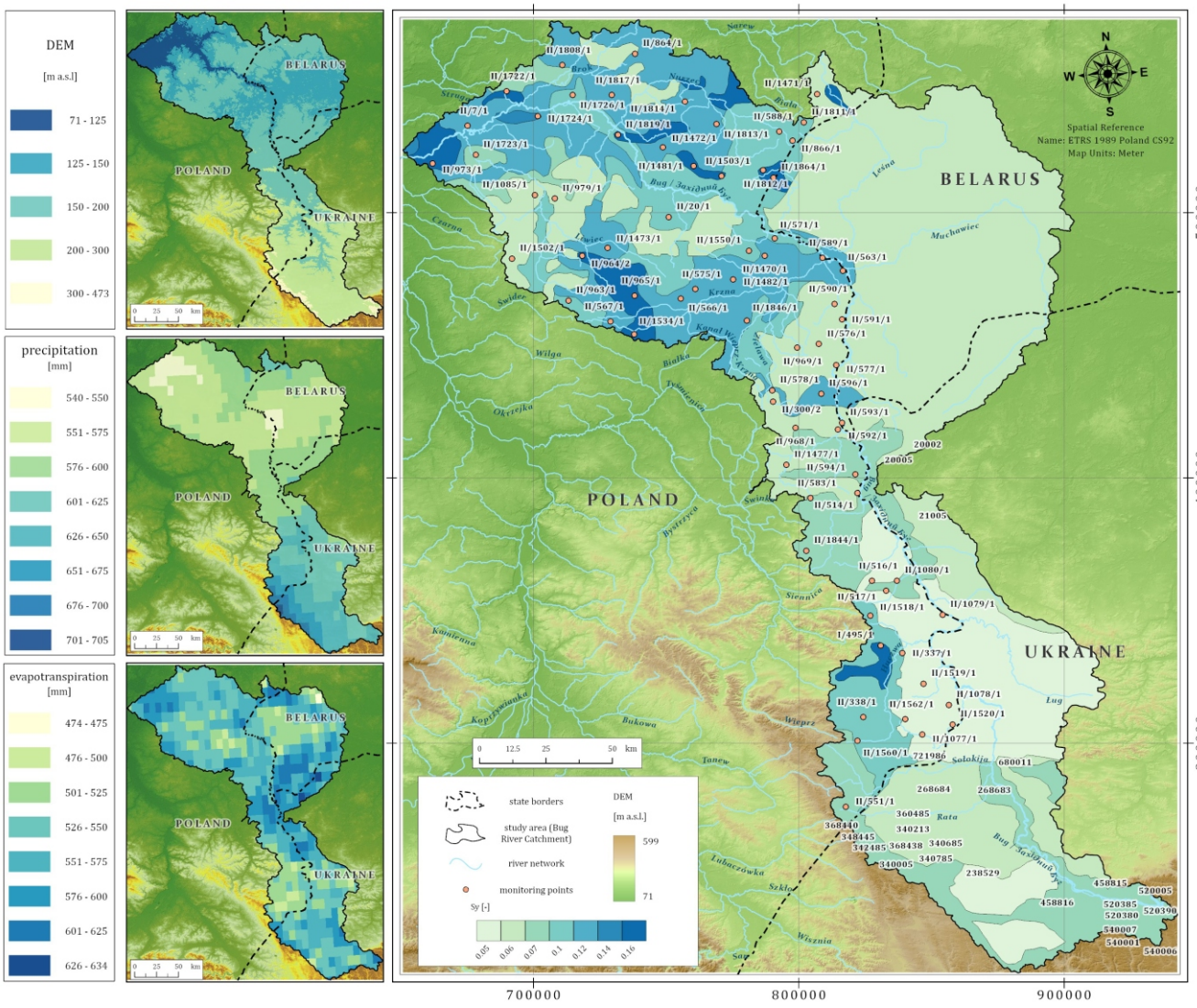

Fig. 1. Location and characteristics of the study area: digital elevation model (DEM, top left), average annual precipitation for 2012–2023 (middle left), average annual evapotranspiration for 2012–2023 (bottom left), and the location of monitoring points and spatial distribution of specific yield (Sy) (right)

specific area, improving spatial resolution and reducing noise compared to traditional spherical harmonic (SH) methods. In most mascon solutions, TWS anomalies are derived directly from observed accelerations and changes in the distance between satellites, eliminating the need for an indirect conversion between SH coefficients and TWS (Watkins et al., 2015; Landerer et al., 2020). This is particularly useful in analysing regional water storage changes. Mascons enhance spatial resolution by allowing the detection of mass variations more precisely over small areas (e.g., river basins or aquifers) compared to global SH. Mascon solutions are currently more widely exploited in regional analyses than data based on SH coefficients (e.g., Scanlon et al., 2016; Ran et al., 2018; Jing et al., 2019; Velicogna et al., 2020).

In the CSR RL06.3, TWS anomalies were calculated using 40,962 equal-area hexagonal or pentagonal mascons (Save et al., 2016). In the final dataset, TWS variations were resampled onto regular 0.25° × 0.25° longitude-latitude grids, enhancing coastline representation and facilitating data application for smaller regions. However, the native resolution of CSR RL06.3, determined by the mascon size used for calculations, is 1° × 1° (Save et al., 2016). The data were accessed from the CSR website (https://www2.csr.utexas.edu/grace/RL06_mascons.html – accessed on January 9, 2025).

EVAPOTRANSPIRATION DATA

For ET, we use SSEBop (Operational Simplified Surface Energy Balance) model data based on Visible Infrared Imaging Radiometer Suite (VIIRS) thermal imagery, updated every 10 days (Savoca et al., 2013; Senay, 2018). The unique feature of the SSEBop model is that it uses a pre-defined, seasonally and spatially dynamic surface psychrometer parameter to calculate ET fractions (ETf) as the difference between observed land surface temperature (dry-bulb) and a cold/wet boundary condition (wet-bulb) using the principle of satellite psychrometry (Senay, 2018). The dataset is produced by estimating latent heat flux through surface energy balance principles. This robust model is instrumental in analysing the spatiotemporal patterns of water use across land surfaces. The advantage of this product is its high resolution (1 km × 1 km, which corresponds to around 0.01° × 0.01° grids) and good quality in the study area, verified

with *in situ* data (Somorowska, 2021). The data were obtained from the website (https://earlywarning.usgs.gov/fews/product/460 – accessed on January 9, 2025).

PRECIPITATION DATA

For precipitation, we use E-OBS daily gridded meteorological data (Cornes et al., 2018). E-OBS is a comprehensive observational dataset covering various surface climate variables, including daily precipitation, temperature, sea level pressure, wind speed, relative humidity and global radiation. These parameters are derived from in-situ measurements collected from national data archives and then resampled using statistical interpolation to create a regular grid with sizes of 0.1° × 0.1° or 0.25° × 0.25° (Haylock et al., 2008; Klok and Klein Tank, 2008). E-OBS was originally developed to support the validation of Europe-wide climate model simulations generated under the European Union's ENSEMBLES project (van der Linden and Mitchell, 2009). Although E-OBS continues to play a vital role in model validation (Nikulin et al., 2011; Min et al., 2013), it is also widely utilized for general climate monitoring across Europe (van Oldenborgh et al., 2016; Lavaysse et al., 2017), and studies on climate impacts (Fibbi et al., 2016; Duveiller et al., 2017). The data are available for Europe from 1950 to the present and are continuously updated not only for subsequent days but also for the stations, the number of which is steadily increasing. Here, we use the most recent version of E-OBS, 30.0e, given in 0.1° × 0.1° grids, released in September 2024 and available at: https://surfobs.climate.copernicus.eu/dataaccess/access_eobs.php#datafiles (accessed on 9 January 2025).

RUNOFF DATA

The hydrological data used in this study to estimate river discharge were obtained from in-situ measurement stations. The study utilized monthly river discharge series from 2012 to 2023. The source data, daily river discharge for 30 gauging stations, was retrieved from the collections of the Institute of Meteorology and Water Management in Poland and the Institute of Hydrometeorology of Ukraine. The data were obtained from the website (https://danepubliczne.imgw.pl/datastore – accessed on 9 January 2025). The river discharge was converted into runoff per square kilometre of the catchment area.

METHODS

GRACE DATA PROCESSING

Due to the original size of the mascon (1° × 1°) in the CSR RL06.3 solution, adjacent 0.25-degree grids showed almost identical TWS anomaly values, making analyses on such a dense grid redundant. Therefore, to reflect the actual temporal resolution of GRACE resulting from the size of the mascon, we resampled the 0.25-degree grids to 1-degree grids using three-dimensional linear interpolation. Accordingly, all other input data (P, ET, and R), originally available at higher spatial resolutions, were aggregated to the 1° grid used consistently throughout the study.

A commonly known limitation in the use of GRACE data is the one-year gap between the end of the GRACE mission and the beginning of the GRACE-FO operation. Various methods have been proposed to fill this gap, employing statistical techniques, more advanced approaches utilizing machine learning, and exploiting supplementary data (e.g., Forootan et al., 2020; Li et al., 2020; Sun et al., 2021; Gyawali et al., 2022). In this study, we use an autoregressive integrated moving average (ARIMA) for prediction of missing months, which is effective for series where the seasonal signal is dominant (Box et al., 2016). Other occasional data gaps in GRACE-based TWS series (of a length of 1 or 2 months) were filled using linear interpolation.

COMPUTATION OF SCALING FACTORS

GRACE solutions based on SH coefficients require low-pass filtering due to vertical stripes on the TWS maps, which are high-frequency noise resulting from the polar-orbiting satellite constellation. However, the effect of filtering is excessive smoothing of the signal, which leads to noticeable attenuation of the TWS anomaly amplitudes and removal of the local specificity of TWS changes (Vishwakarma et al., 2016; Hu et al., 2021). Even after applying scaling factors from popular land surface models or global hydrological models, the GRACE signal still shows considerable attenuation of both seasonal and long-term cycles (Long et al., 2015).

An existing solution to this problem is the use of a mascon approach, where TWS anomalies are directly calculated in each mascon from observations of the changes in distance between the satellites, without the intermediate step of determining SH coefficients. However, in the study area, TWS data obtained from the CSR mascon solution do not show the same spatial heterogeneity as TWS-WB. This means that the mascon approach does not fully capture the signal observed in estimates based on the water balance approach. The limitation of the GRACE data, in this case, lies not in the processing method of the observations, but in the temporal and spatial resolution of the measurements, which cannot be enhanced without supplementary information from other sources. Therefore, we considered it essential to perform additional scaling, ensuring that the conclusions drawn in the subsequent analysis – comparing TWS-GRACE and TWS estimations based on water balance component observations – would be based on normalized data.

The determination of the scaling factor is not intended to restore signal loss in GRACE data resulting from low-pass filtering, which, in this case, should not be an issue due to the use of mascon solutions (Longuevergne et al., 2010). Scaling is performed to reconcile changes in TWS-GRACE with those modelled based on the water balance approach. The scaling factor for each grid cell can be computed by least square fit between spatially averaged TWS-GRACE data and unfiltered modelled TWS-WB anomalies obtained from observed precipitation, evapotranspiration, and in-situ streamflow data. The scaling factors derived in this way for each grid cell were applied by multiplying to correct the TWS-GRACE data. The values of the scaling factors indicate to what extent GRACE underestimates the TWS signal obtained from the water balance approach.

Fusing GRACE data into the terrestrial water budget

The month-to-month TWS-WB change (TWS-WB) is determined by the variability of hydrological fluxes, which are interconnected through the water balance equation:

$$\frac{dS}{dt} \quad P \quad R \quad ET \qquad [1]$$

where: *dS/dt* – the monthly TWS change (TWS) (mm/month); *P* – the monthly precipitation (mm/month); *R* – the streamflow (mm/month); *ET* – the monthly evapotranspiration (mm/month). *P* and *ET* were obtained using satellite products assimilated with model data, while R was derived from in-situ measurements.

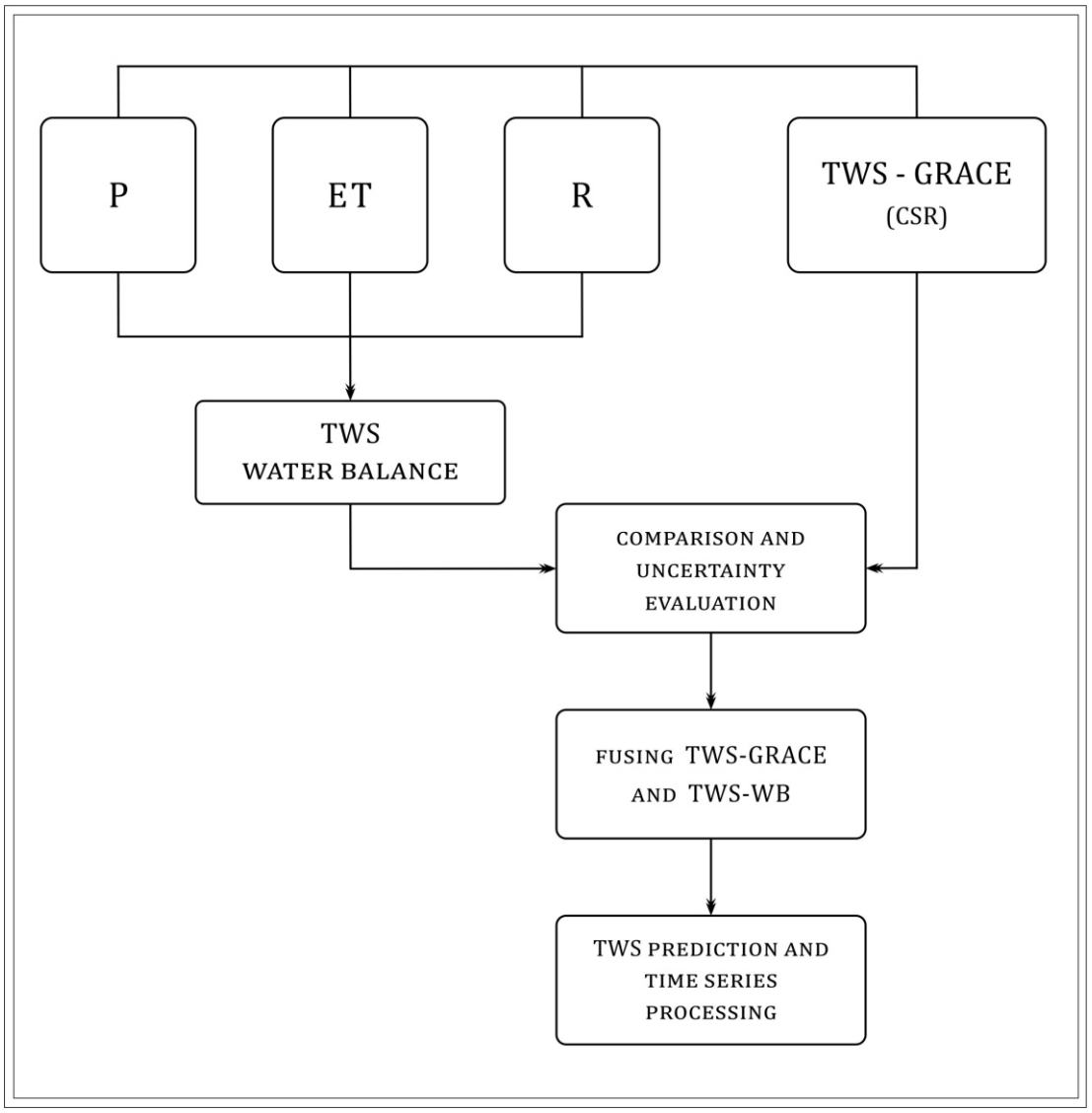

Fig. 2. Flowchart of the analysis of TWS-GRACE, TWS-WB, and the fusion of TWS-GRACE and TWS-WB conducted in this study

The month-to-month TWS-GRACE change (TWS-GRACE) is determined based on TWS anomalies (in mm) provided by GRACE for the period 2012–2023 for a specific month (*t*):

$$\frac{dS}{dt} \quad \frac{TWS_{t\ 1} \quad TWS_{t\ 1}}{t} \qquad [2]$$

The relationship between the TWS-WB and the TWS-GRACE at grid scale was established using a multidimensional linear regression model. This model links the dependent variable (*Y*) – the variable to be predicted – with the independent variables (*X*), derived from the set of observations:

$$Y \quad XH \qquad [3]$$

where: *Y (n* × *g)* – a matrix with *n* rows (one for each month) and *g* columns (one for each grid cell in the Bug Basin). The predictor matrix *X (n* × *d)* has *n* rows (one for each month) and *d* columns containing *P*, *ET*, *R* and TWS-GRACE. *H (d* × *g)* – the prediction matrix. This calculation is preceded by the standardization of data required for the predictor matrix *X*. Typically, global products are available in grid cell formats with varying spatial resolutions. For the purposes of the analysis, the values of *P*, *ET* and *R* were adjusted to match the spatial resolution of TWS-GRACE (1° × 1° grid).

Dimension reduction is crucial for multivariate regression analysis, achieved using Partial Least Squares Regression (Vishwakarma et al., 2021). This analysis aims to regress on the Principal Components (PCs) of measurements that strongly correlate with the target signal (Preisendorfer, 1988).

To evaluate the accuracy of the final product – combined TWS derived from TWS-GRACE and water balance components – commonly used statistical indicators were applied, including the root mean square error (RMSE) and the Pearson correlation coefficient (CC).

Figure 2 presents a flowchart of the process of fusing TWS-GRACE and TWS-WB, as well as the analysis of the results obtained.

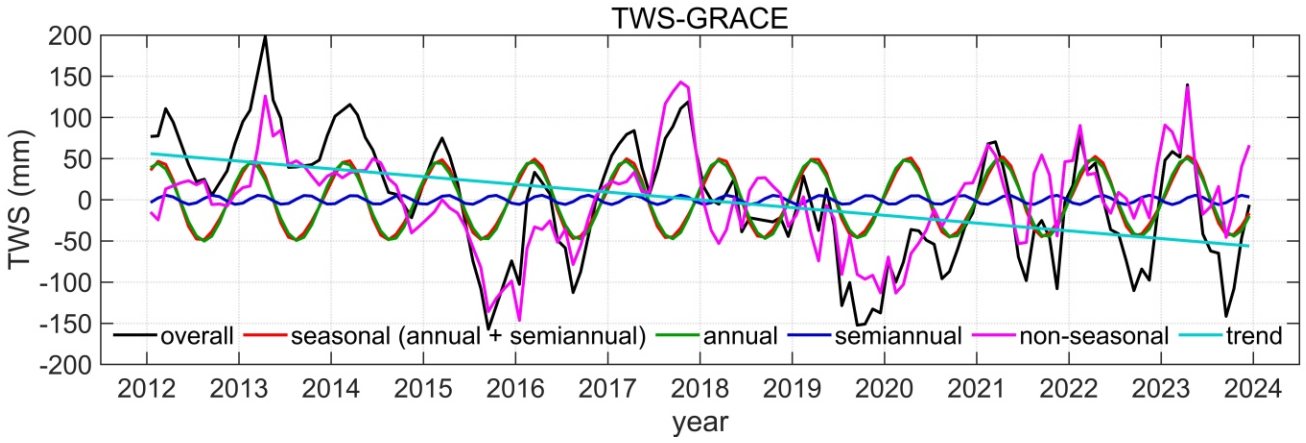

Fig. 3. Example of processed TWS-GRACE series – overall series, seasonal (sum of annual and semiannual oscillation) oscillations, annual oscillations, semiannual oscillations, nonseasonal variations, linear trend

METHODS OF TIME SERIES PROCESSING

Because all datasets were available for different time periods, we limit our research to the common period between January 2012 and December 2023. All the series were also sampled to monthly intervals.

A detailed analysis of TWS series consists of the study of trends, seasonal oscillations (sum of annual and semiannual signal) and non-seasonal variations. For this purpose, the TWS series for each grid were decomposed into appropriate components:

$$TWS \quad TWS_{trend} \quad TWS_{seasonal} \quad TWS_{non\ seasonal} \qquad [4]$$

Trends and seasonal signal were computed together by fitting a seasonal model to the series using the least-squares method. This model comprised a first-degree polynomial defining the trend and the sum of sine waves with periods of one year and half a year, which determined the seasonal oscillation (sum of annual and semiannual signal), according to the following formula:

$$y\ t \quad a \quad b\ t\ t_0 \quad c\cos \quad t\ t_0 \quad d\sin \quad _a\ t\ t_0 \quad e\cos \quad _s\ t\ t_0 \quad f\sin \quad _s\ t\ t_0 \qquad [5]$$

where: y – the value of the series for the time $t = 1, \ldots, 144$ (number of months), a – the intercept, b – a trend coefficient, c, d, e, f are coefficients of the fitted sinusoids, t_0 – a reference epoch (first month of analysis, here January 2012), and $_a$, $_s$ – annual and semiannual frequencies, respectively.

Non-seasonal changes were further obtained by removing trends and seasonal signals, thus capturing all other variations with periods both longer and shorter than seasonal changes. Figure 3 illustrates example TWS-GRACE series for the grid with the centre coordinates 51.5°N, 24.5°E, highlighting the overall series (the original series without separation into seasonal and non-seasonal oscillations), seasonal components (the sum of annual and semiannual signals), annual oscillations, semiannual oscillations, non-seasonal changes, and the linear trend. The plot indicates that seasonal oscillation is primarily influenced by the annual signal, as the amplitudes of the semiannual variations are several times smaller. Consequently, this study will concentrate on the annual oscillation.

The annual signal is further analysed by examining phasor diagrams, depicting the amplitudes and phases of the oscillation in relation to a chosen reference date (in this study the reference date is January 2012, marking the beginning of our dataset). The amplitude (*Amp*) and phase (*Ph*) of annual oscillation were computed for each series by employing coefficients c and d from a fitted model:

$$Amp \quad \sqrt{c^2 \quad d^2} \qquad [6]$$

$$Ph \quad \tan^{1} \frac{d}{c} \qquad [7]$$

To conduct a comprehensive analysis of non-seasonal variations in TWS, we divided them into short-term changes (with periods shorter than two years) and long-term changes (with periods longer than two years) by applying a high-pass Butterworth filter (Butterworth, 1930). Figure 4 shows example TWS-GRACE series for a grid centred at 51.5° N, 24.5° E, highlighting the distinctions between non-seasonal, non-seasonal long-term, and non-seasonal short-term changes.

To analyse the predominant oscillations within the TWS series, we utilize amplitude spectra derived through the application of the fast Fourier transform (FFT). The FFT method facilitates the conversion of signals from their time-domain representation to the frequency-domain representation, enabling the investigation of signal properties such as frequency composition (Brigham and Morrow, 1967). The amplitude spectrum obtained by the FFT process shows the magnitudes of the various frequency components present in the input data and makes it possible to find the most significant frequencies in the signal and their contribution to the overall behaviour of the signal.

RESULTS

SCALING FACTOR FOR TWS-GRACE FROM THE WATER BALANCE REGRESSION MODEL AT THE GRID CELLS

The original mascon solution from CSR is available on a 0.25° × 0.25° grid; however, the actual spatial resolution, determined by the size of the mascon applied by CSR, is 1° × 1°. This means that GRACE data do not contain physical information at a spatial scale finer than the original GRACE resolution. To en-

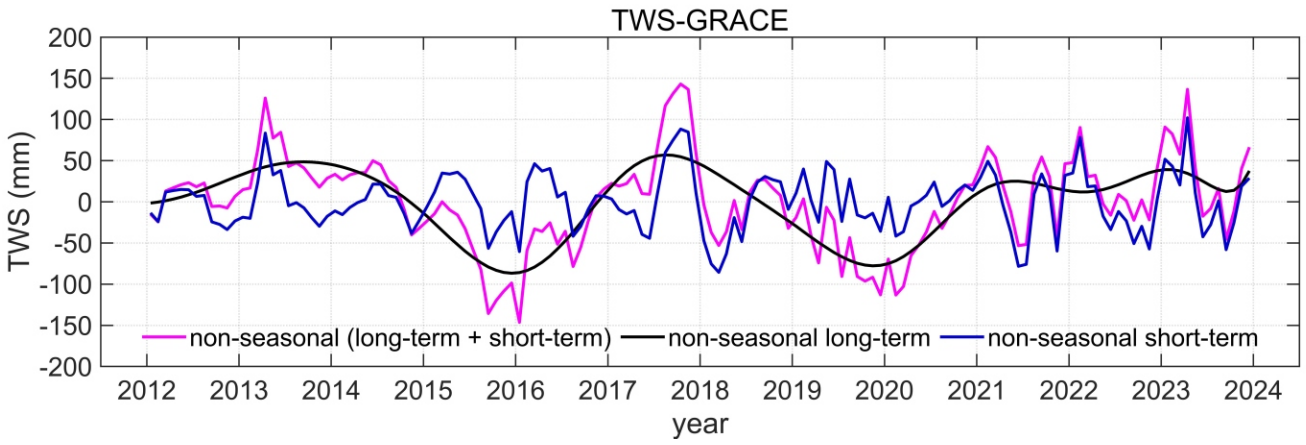

Fig. 4. Example of processed non-seasonal TWS-GRACE series – non-seasonal, non-seasonal long-term and non-seasonal short-term

hance the spatial resolution of GRACE products, it is necessary to incorporate additional high-resolution information. In this study, we used a water balance model, where TWS-WB estimates are a function of the variables P, ET and R. Both TWS-GRACE and TWS-WB are analysed here in 1° × 1° grids even though the data for the water mass balance equation are provided at a higher spatial resolution than GRACE.

To illustrate the effect of the low resolution of TWS-GRACE, even on a 1°×1° grid, TWS variations were compared with TWS-WB using standard deviations. The calculated standard deviation values for the TWS-GRACE and TWS-WB time series for the 2012–2023 period in the Bug Basin show clear spatial differences (Fig. 5). TWS-GRACE (Fig. 5A) does not exhibit local features but is characterized by zonality resulting from the method of data interpolation. In contrast, TWS-WB (Fig. 5B) displays spatial heterogeneity, logically reflecting the non-uniformity of water cycle transformations due to surface properties.

The scaling factors determined in this study, derived from the comparison of water balance estimates and TWS-GRACE changes, exhibit a clear spatial tendency (Fig. 6). Relatively

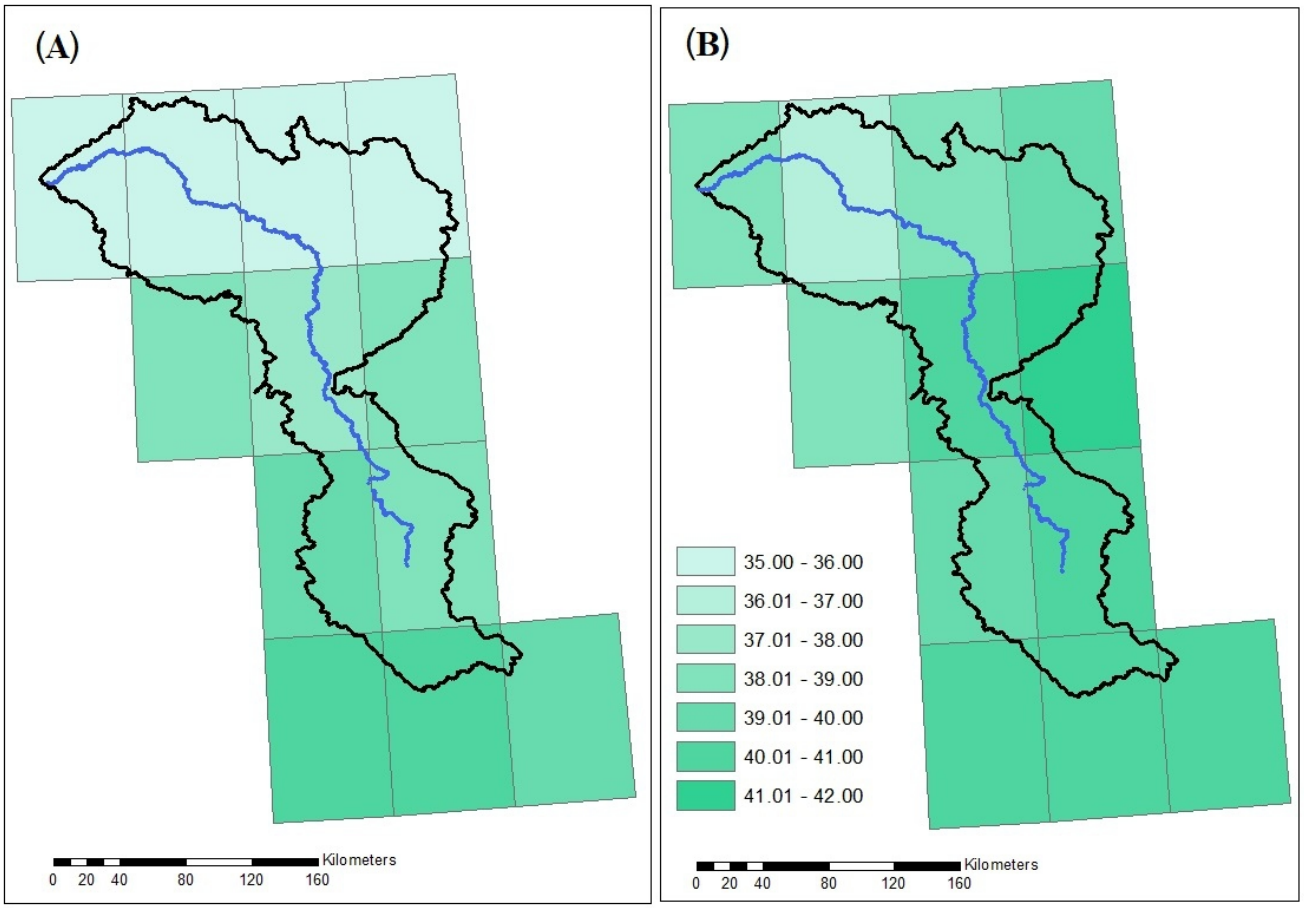

Fig. 5. Standard deviations (in mm) of TWS changes over the period between January 2012 and December 2023 for the Bug River basin: (A) TWS-GRACE data from CSR mascon solution and (B) TWS-WB calculated from observational data of water balance components

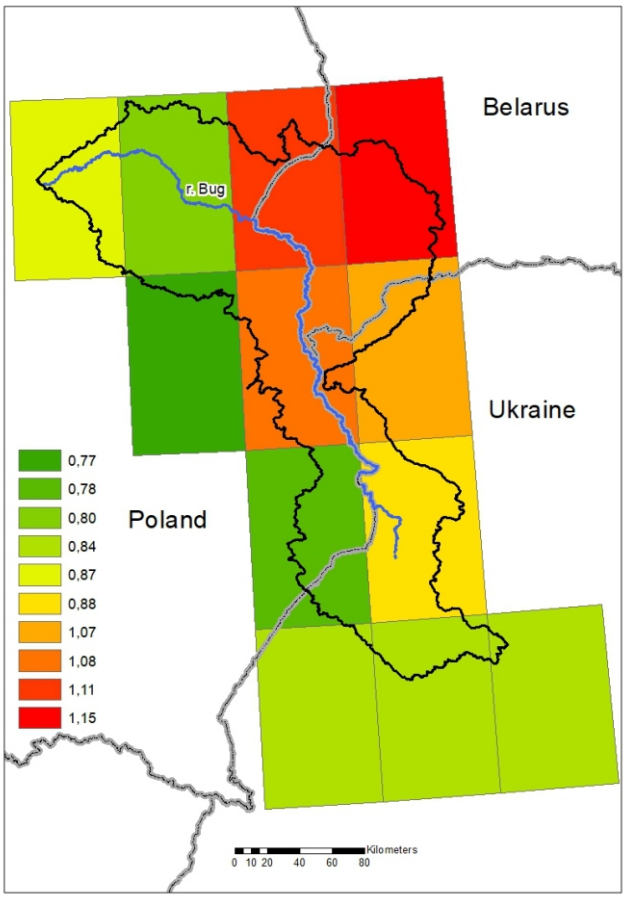

Fig. 6. Scaling factors computed based on comparison between TWS-WB and TWS-GRACE

higher values of scaling coefficients (>1.0) are observed in grid cells located in flat areas with optimal conditions for land-based retention of rainfall water. In these areas, the variability of the observed TWS-WB is highest, which, however, is not the case for TWS-GRACE, thus requiring a significantly higher value of scaling factor. In the upper Bug River in the upland areas the scaling factor values are the lowest (<0.84), which indicates that in these regions the variability of TWS-GRACE is equal or even higher than in the case of TWS-WB.

The scaling coefficient does not significantly affect the R^2 value between TWS-GRACE and TWS-WB, but it causes a proportional adjustment of the amplitudes derived from GRACE in relation to those estimated based on the water balance approach. The TWS-GRACE values after scaling improved the consistency with TWS-WB, as indicated by a lower RMSE. For the entire Bug River basin, the RMSE is 34.7 mm/month for TWS-GRACE changes alone and 34.0 mm/month for TWS-GRACE after applying the scaling coefficient. The greatest improvement is observed in the upper course of the river in the hilly area (from 38.0 to 36.9 mm/month). In the lower, lowland part of the Bug Basin, the TWS-GRACE changes with the scaling coefficient show only a slightly smaller discrepancy with TWS-WB than the TWS changes without scaling (35.7 and 35.8 mm/month, respectively).

COMPARISON OF TWS-GRACE AND TWS-WB

Figure 7 shows the TWS-GRACE and TWS-WB time series averaged over the Bug River Basin for the period 2012–2023, while Figure 7 shows the changes in the corresponding TWS series averaged for each subsequent year. During the period analysed, both TWS-GRACE and TWS-WB series show a downward trend in annual values (Fig. 8), with the long-term average TWS for the Bug River Basin being –1.78 mm/year according to GRACE data and –7.58 mm/year according to the

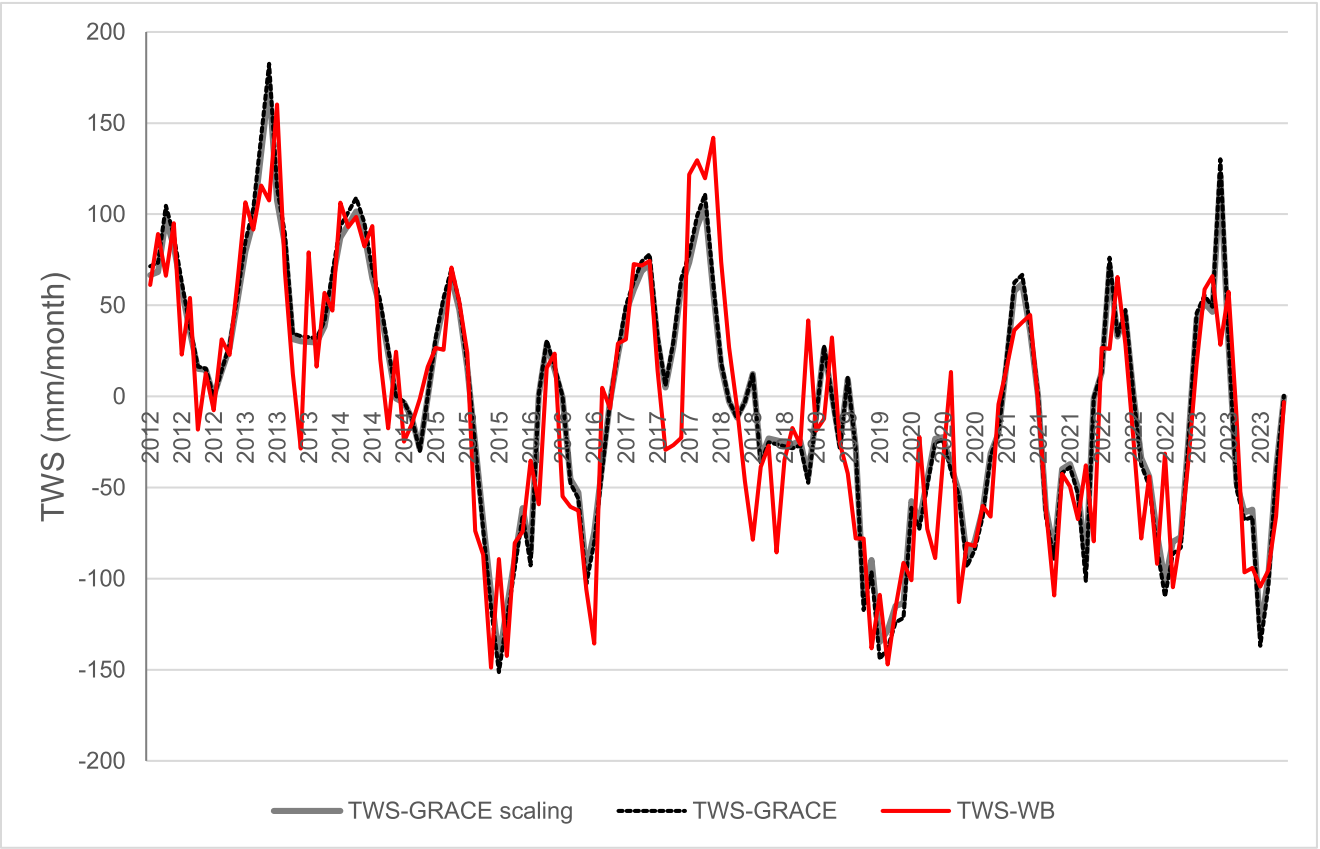

Fig. 7. Time series of TWS-GRACE (with and without scaling factors) and TWS-WB averaged over the area of River Bug Basin for the period between January 2012 and December 2023

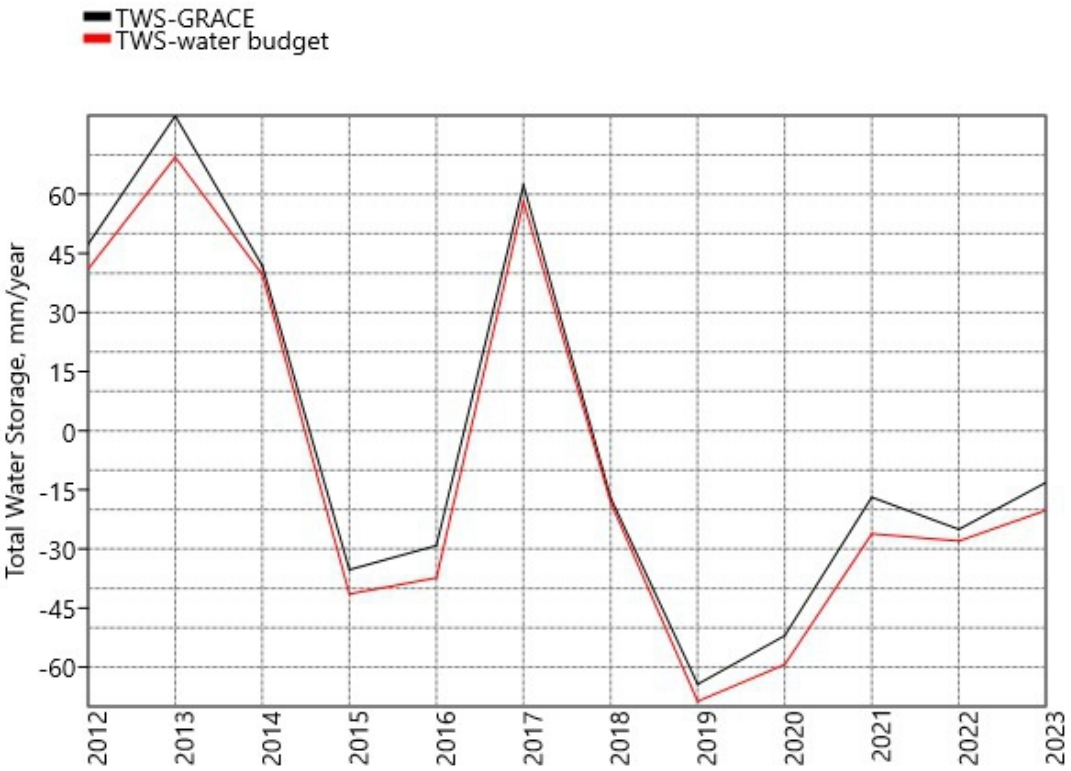

Fig. 8. Changes in TWS-GRACE and TWS-WB averaged for each subsequent year

water budget approach, with standard deviations of 47.2 and 47.0 mm/year, respectively. The highest annual average of TWS (>60 mm/year) was recorded in 2013 and 2017, while the lowest (<–50 mm/year) occurred in 2019 and 2020.

The significance and magnitude of the downward trend varies depending on the month (Table 1). A slightly higher intensity of the decrease in the warm season (from April to September), when ET prevails over P, compared to the cold season (from October to March) is shown only by TWS-GRACE. Moreover, TWS-GRACE is generally characterized by a higher trend significance than TWS-WB. The highest rate of decline is observed in summer and autumn for both series, with the peak decrease for TWS-GRACE occurring in June and September, while for TWS-WB, it occurs in October.

Interesting results were obtained by comparing month-to-month changes of TWS-GRACE (TWS-GRACE) and changes in land retention (TWS-WB; Fig. 9). A negative retention value indicates a water deficit, i.e. the dominance of ET and R over P. Both time series show a division into a dry period (from April to September) with negative values, i.e. a decrease in water resources, and a wet period (from October to March) – with positive values. Clearly greater discrepancies between TWS-GRACE and TWS-WB are observed in the dry period, with a maximum in June, which may indicate greater uncertainty of GRACE measurements at negative TWS values, i.e., when there is less water.

To analyse the consistency between TWS-GRACE and TWS-WB, we drew scatter plots and calculated the coefficient of determination (R^2) between the time series averaged for the entire Bug River Basin, as well as for the Upper Bug and Lower Bug regions (Fig. 9). The results show generally good agreement between the series obtained from GRACE data and from

Table 1

Trend of TWS changes in the Bug River Basin from 2012 to 2023 for each month

Month	Coefficient of regression		Linear regression equation		R^2	
	TWS-GRACE	TWS-WB	TWS-GRACE	TWS-WB	TWS-GRACE	TWS-WB
1	–5.94	–8.32	–5.9378x + 60.512	–8.32x + 79.958	0.15	0.26
2	–4.65	–5.11	–4.6475x + 75.457	–5.1133x + 68.758	0.11	0.14
3	–9.31	–5.62	–9.3135x + 112.17	–5.6183x + 83.571	0.38	0.16
4	–6.11	–9.36	–6.1147x + 95.639	–9.3645x + 92.142	0.12	0.33
5	–7.16	–8.02	-7.1643x + 74.063	–8.016x + 63.44	0.46	0.18
6	–10.50	–7.82	–10.5x + 55.772	–7.8171x + 27.874	0.62	0.30
7	–9.22	–7.64	–9.2227x + 24.568	–7.6434x – 5.9356	0.42	0.45
8	–7.68	–7.11	–7.6789x + 7.1803	–7.1079x – 20.654	0.21	0.21
9	–10.47	–7.95	–10.471x + 12.666	–7.946x + 12.668	0.26	0.14
10	–9.82	–10.64	–9.8168x + 21.534	–10.636x + 30.174	0.26	0.23
11	–9.06	–9.90	–9.0576x + 29.177	–9.8993x + 41.24	0.23	0.29
12	–6.14	–7.80	–6.1421x + 34.317	–7.8002x + 55.12	0.16	0.17

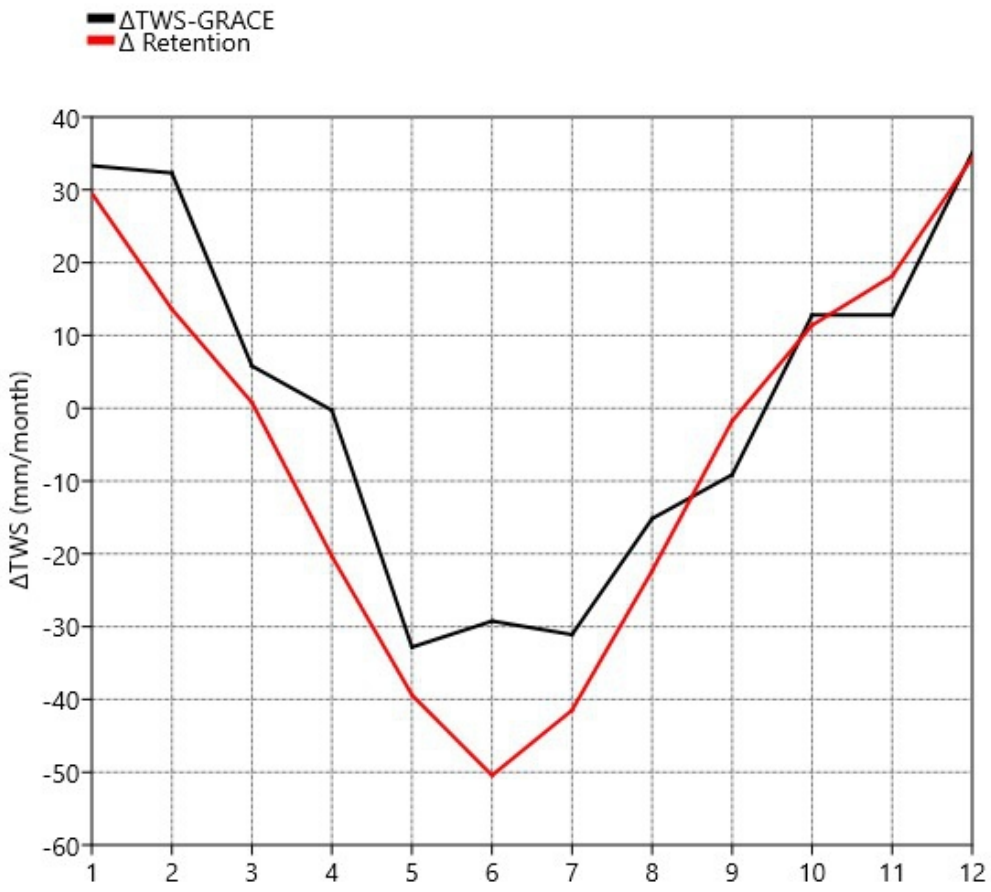

Fig. 9. Dynamics of monthly TWS-GRACE and TWS-WB for the period between January 2012 and December 2023

the water balance equation. The R^2 is 0.77, 0.73, and 0.76 for the entire Bug River Basin, Upper Bug, and Lower Bug, respectively (Fig. 10). Figure 10 also corroborates that scaling the GRACE data has a greater impact on the results in the Upper Bug, whereas for the Lower Bug, the TWS-GRACE values before and after scaling are almost identical. The agreement between TWS-GRACE and TWS-WB is also slightly higher for the lower stretch of the river.

In the remainder of this section we analyse the correlation coefficients between TWS-GRACE and TWS-WB in individual years (Fig. 11) and months (Fig. 12) separately for the entire Bug River basin, its upland (upper) and lowland (lower) parts. For the Upper Bug, we observed a slightly lower correlation than for the Lower Bug. Considering that TWS changes in the Upper Bug are more sensitive to precipitation changes compared to the Lower Bug, and that the precipitation variability in the Upper Bug is high, it can be concluded that the lower agreement between the GRACE data and the estimates from the water balance equation is likely due to the inability to capture short-term precipitation events with the monthly GRACE measurement interval. Furthermore, there is a noticeable decrease in the correlation coefficient in 2018 and 2020. In the first case, this was probably a result of the interruption of GRACE observations and the uncertainty associated with filling in the missing data. In 2020, the low correlation was due to months with extreme precipitation and correspondingly high TWS-WB values, which were not captured in the GRACE measurements.

The correlation analysis for individual months indicates slightly worse agreement between TWS-GRACE and TWS-WB in the Upper Bug than in the Lower Bug, particularly in February and June, when the correlation coefficient drops below 0.7 (Fig. 12). In these months, the largest discrepancies in precipitation between the Upper and Lower Bug are observed, which are also evident in the TWS-WB estimates. However, due to the low temporal and spatial resolution, the TWS-GRACE measurements seem to fail to capture these fluctuations, leading to increased discrepancies with respect to the water balance approach. The smallest disparity between the results for the upper and lower stretches of the river was observed in the winter months, when the TWS values are highest (see Fig. 9). For these months, we also generally observe the highest agreement between TWS-GRACE and TWS-WB, both for the whole river basin and for its upper and lower stretches.

COMPARISON OF TWS-GRACE SERIES WITH AND WITHOUT FUSION WITH P, ET AND R DATA

The assimilation of P, ET, and R data into TWS-GRACE helped compensate for the errors in the GRACE solution by incorporating higher-resolution spatial information. The comparison between the TWS-GRACE series without fusion and the TWS-GRACE corrected through fusion with P, ET and R data averaged for the entire Bug River Basin is shown in Figure 13. Table 2 illustrates the comparison of the minimum, maximum,

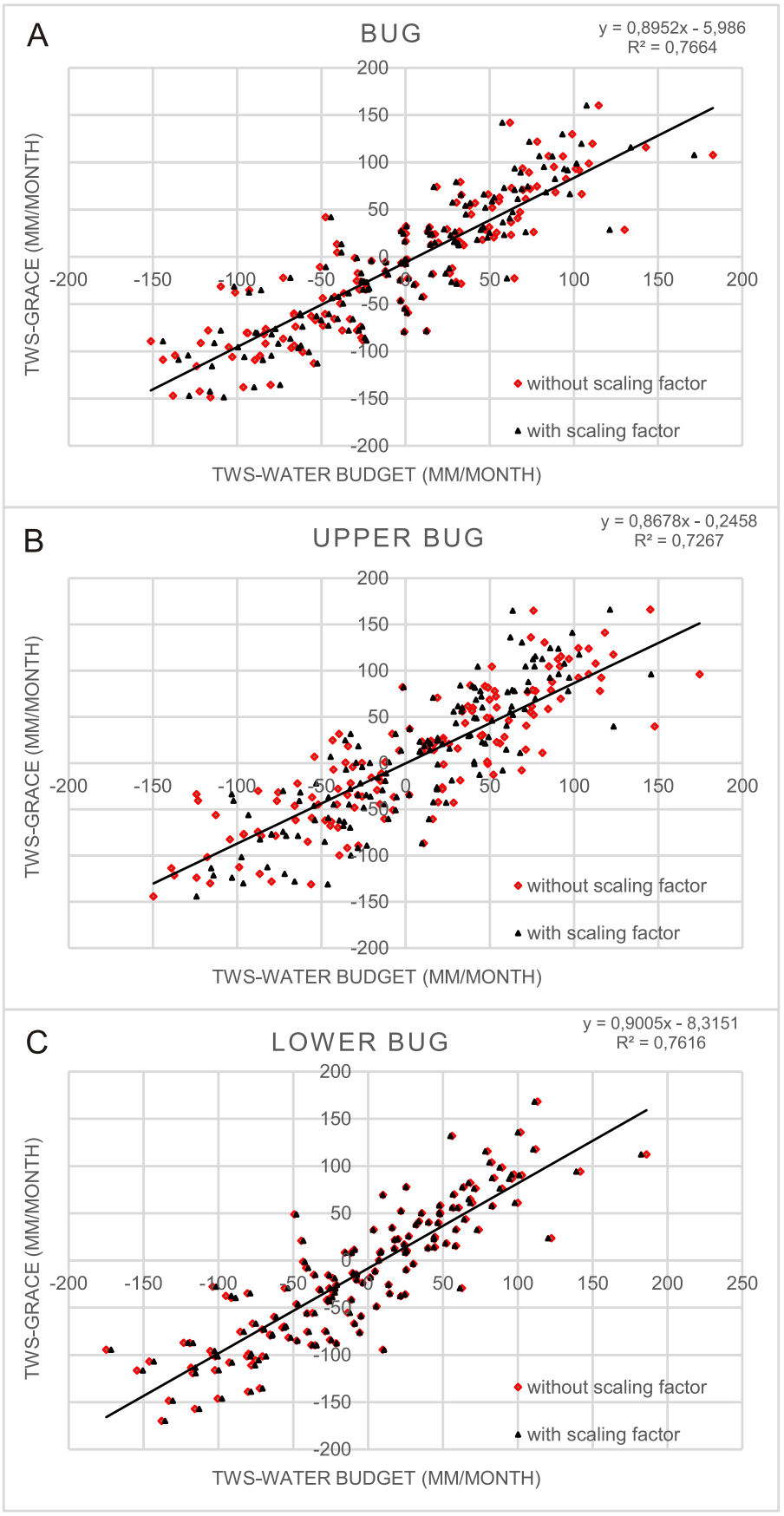

Fig. 10. Scatterplots of TWS-GRACE and TWS-WB for the entire Bug River basin (A), Upper Bug River Basin (B) and Lower Bug River Basin (C) for the period between January 2012 and December 2023, together with coefficients of determination (R^2) and regression equation

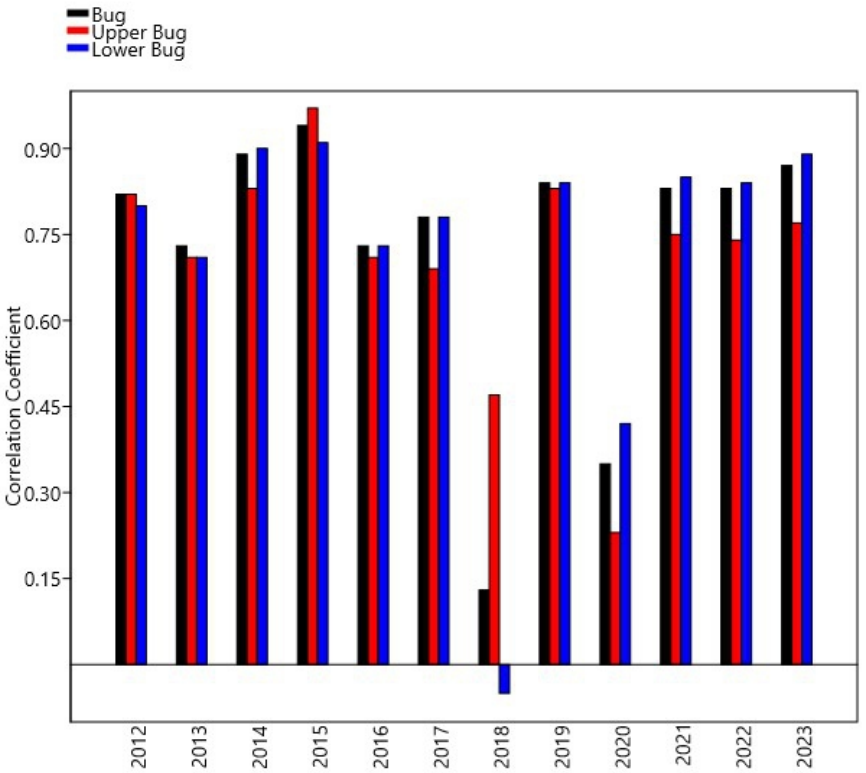

Fig. 11. Correlation coefficients between TWS-GRACE and TWS-WB for the entire Bug River Basin, and for the Upper Bug River Basin and Lower Bug River Basin for each year separately

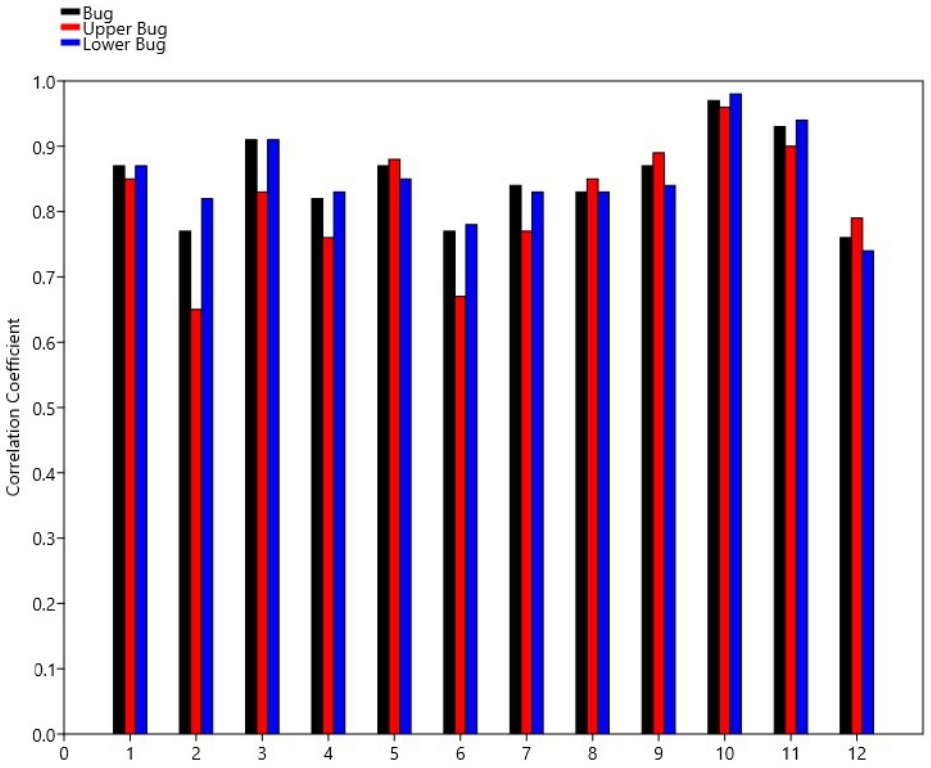

Fig. 12. Correlation coefficients between TWS-GRACE and TWS-WB for the entire Bug River Basin, as well as for the Upper Bug River Basin and Lower Bug River Basin for each month separately

Table 2

The minimum, maximum and average values of TWS-GRACE without and with fusion with P, ET and R data for each year of the period analysed

Year	Minimum			Maximum			Average		
	Fusing TWS-GRACE	TWS-GRACE	Difference	Fusing TWS-GRACE	TWS-GRACE	Difference	Fusing TWS-GRACE	TWS-GRACE	Difference
2012	–1.3	–0.4	–0.9	92.9	104.6	–11.8	46.8	47.3	–0.5
2013	10.4	32.0	–21.6	154.5	182.5	–28.0	77.7	79.9	–2.2
2014	–18.6	–30.1	11.5	104.8	108.9	–4.1	41.0	41.9	–0.9
2015	–128.4	–151.3	22.9	72.2	69.9	2.3	–31.6	–35.3	3.7
2016	–103.1	–102.9	–0.2	27.4	30.8	–3.4	–31.4	–29.2	–2.3
2017	–13.6	6.0	–19.6	143.1	111.1	32.0	64.6	62.4	2.2
2018	–71.1	–47.4	–23.6	74.1	18.5	55.6	–14.9	–17.0	2.1
2019	–139.7	–144.1	4.4	16.7	27.7	–11.0	–66.5	–64.3	–2.2
2020	–98.9	–93.5	–5.4	7.9	–20.2	28.1	–54.5	–52.0	–2.5
2021	–104.3	–101.2	–3.1	56.3	66.7	–10.4	–22.0	–16.9	–5.1
2022	–91.7	–109.7	18.0	62.9	76.2	–13.2	–19.6	–25.0	5.4
2023	–121.6	–136.9	15.4	58.7	130.1	–71.3	–19.3	–13.2	–6.2

and average TWS values for each year of the period analysed. It can be seen from Table 2 that the effects of the fusion in TWS-GRACE are most evident in the reduction of ~16% of the original maximum TWS values (except for the years 2017, 2018 and 2020), which results in a slight (~7%) decrease in the average value.

Figure 14 shows a comparison of TWS-GRACE and TWS-GRACE with data fusion for the dry period, obtained by taking a median of values for the months of April-September over the years 2012–2023. According to the climatic conditions in this geographical zone, TWS is characterized by negative values, as ET losses exceed P. It can be observed from Figure 14 that TWS-GRACE after fusion with P, ET, and R data tends to adopt negative values. The greatest differences between TWS-GRACE with data fusion and TWS-GRACE without data fusion occur in the years 2017 and 2018, during the gap between the end of GRACE operation and the start of GRACE-FO measurements. This demonstrates the validity of filling the missing GRACE data through fusion with P, ET and R data, rather than using ARIMA. Years with noticeable discrepancies between TWS-GRACE with and without fusion also include 2013, 2016 and 2020, during which GRACE observations recorded the lowest TWS values (not exceeding –15 mm/month). For small changes in TWS, the accuracy of GRACE measurements decreases. It is currently believed that changes in water storage anomalies can be detected if their magnitude exceeds 1.5 cm over an area of 200,000 km^2 (Frappart et al., 2018).

In the wet period (October-March), a noticeable difference in results is observed between the GRACE (until 2017) and GRACE-FO (from 2018 onwards) periods (Fig. 15). In the first case, the correction of TWS-GRACE is almost always nega-

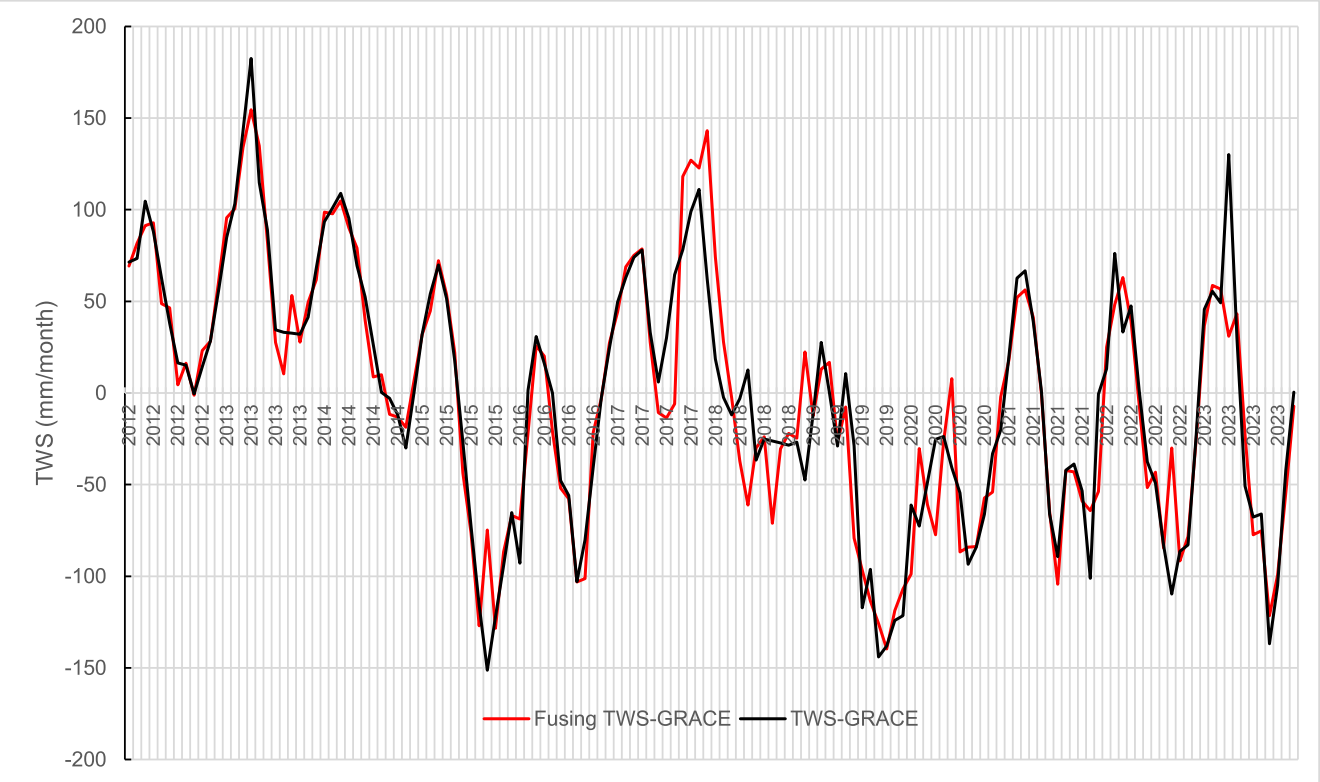

Fig. 13. Time series of original TWS-GRACE and TWS-GRACE values corrected through fusion with P, ET, and R data for the Bug River Basin for the period between January 2012 and December 2023

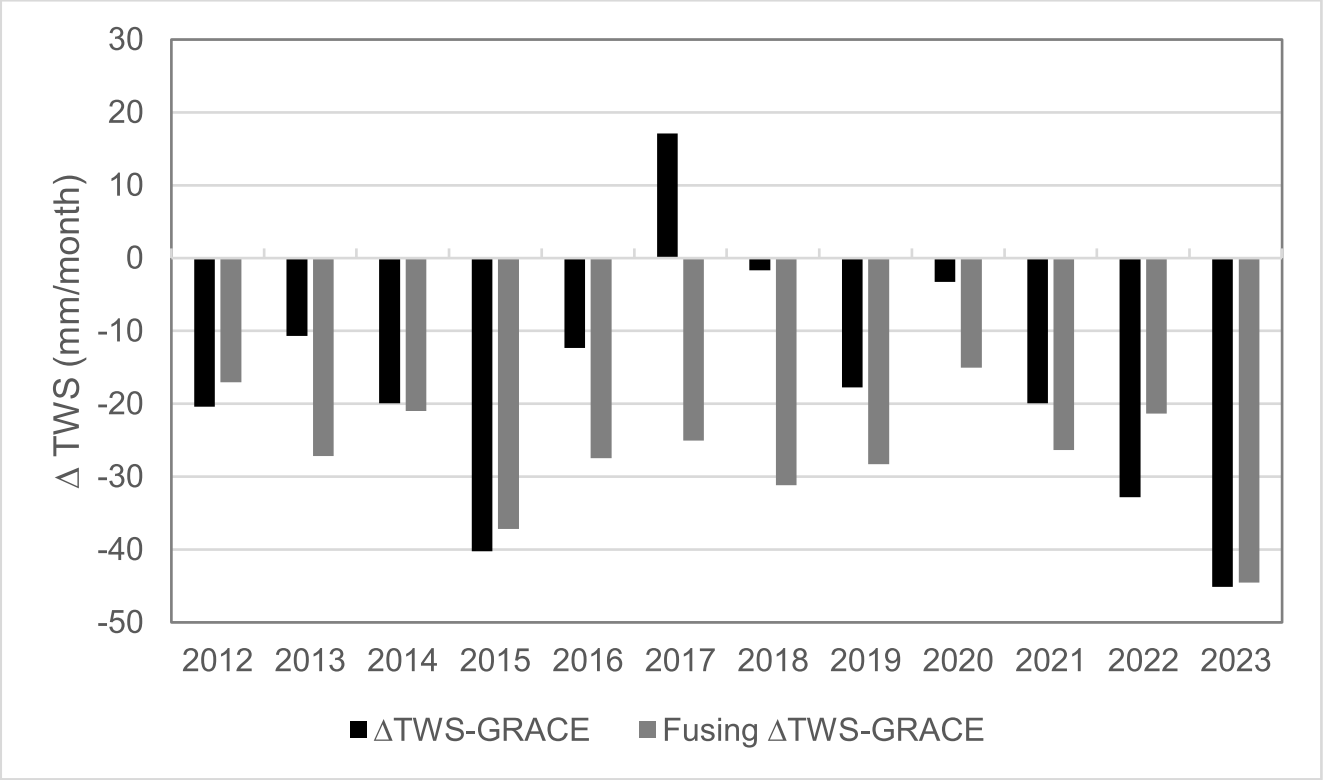

Fig. 14. Comparison of TWS-GRACE and TWS-GRACE after fusion with P, ET and R data for the dry period (April-September) for the Bug River Basin

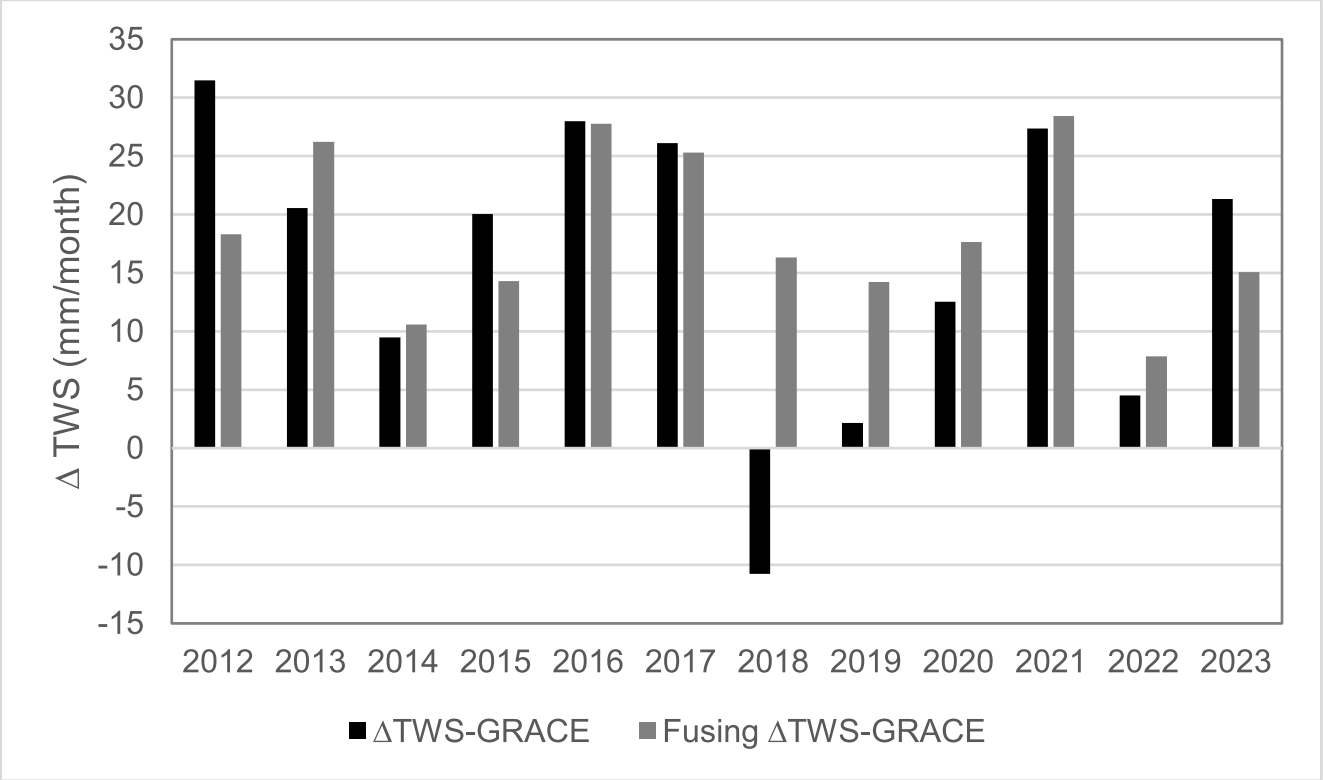

Fig. 15. Comparison of TWS-GRACE and TWS-GRACE after fusion with P, ET and R data for the dry period (October-March) for the Bug River Basin

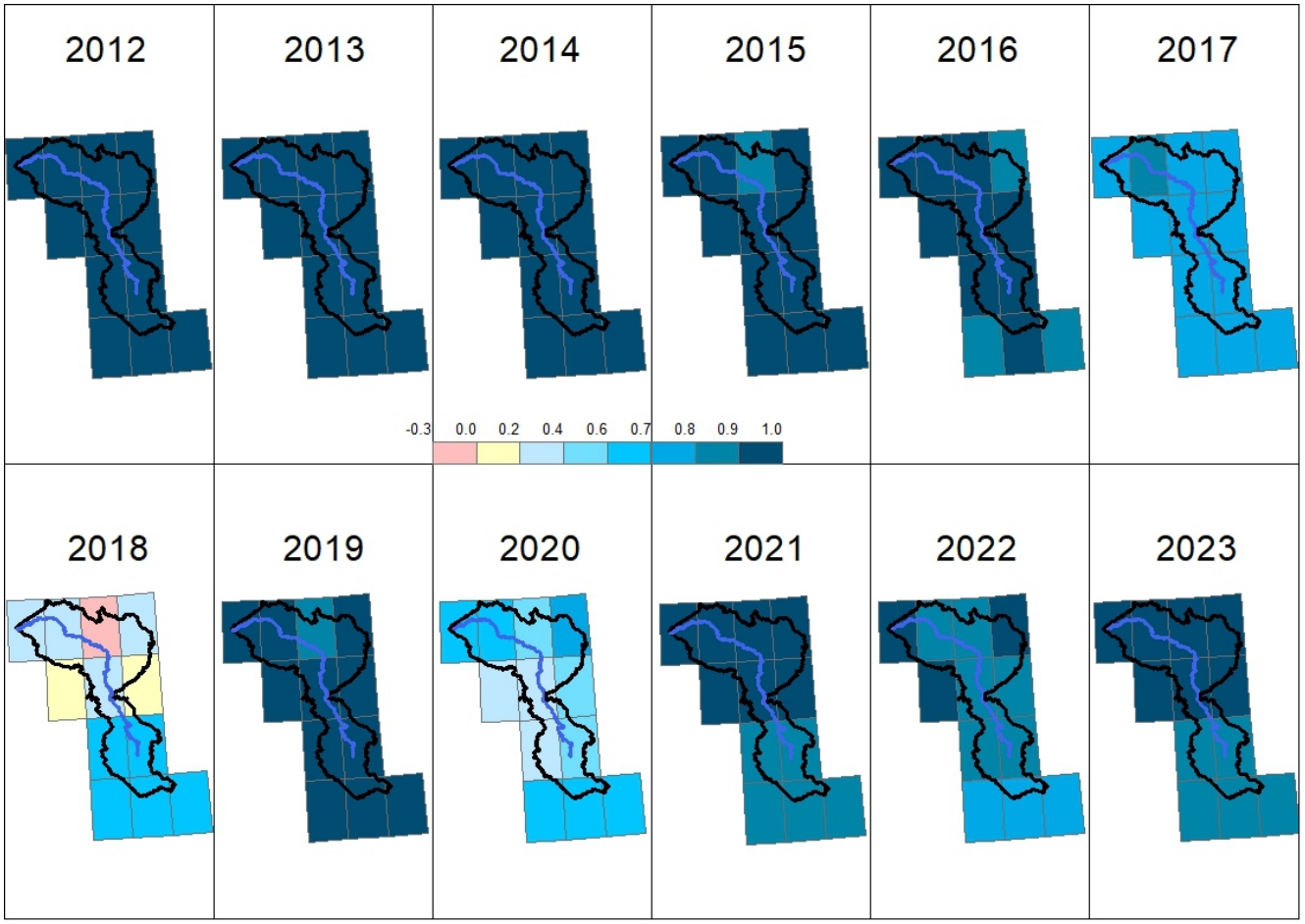

Fig. 16. Correlation coefficients between TWS-GRACE and TWS-GRACE after fusion with P, ET and R data for each grid cell covering the Bug River Basin

tive, whereas during the GRACE-FO mission, it is positive. Again, the largest difference between TWS with and without fusion occurs in the years when observations were interrupted, but in this case, only in 2018. Furthermore, as in the dry period, the issue of GRACE measurement precision becomes apparent. The greatest compensation is required for the year 2019, which has the lowest TWS-GRACE value, falling outside the detection threshold. Overall, verification of TWS-GRACE calculations based on high-resolution P, ET and R data suggests that during the wet period, with larger amplitude changes, this method yields better results than in the dry season.

The spatial correlations between TWS-GRACE and TWS-GRACE after fusion with P, ET and R data are shown in Figure 16. The highest consistency between series was recorded for the entire area during the years 2012–2014, corresponding to the period of the highest quality of GRACE measurements. On the other hand, the years with the lowest correlations include 2017 and 2018, which lacked GRACE measurements. The year 2020 also shows a distinctly lower correlation, further confirming the increased error in GRACE-FO data during that time. Additionally, a slightly worse correlation is noticeable in the upper part of the Bug River watershed in the last three years (2021–2023), suggesting that the scaling factors used in the GRACE solution for this area diverge from the actual water mass redistribution predicted by the water balance equation. Overall, correcting TWS-GRACE using fusion with high-resolution data brings the most benefits during years with poor data quality or unavailability of GRACE measurements, and in the upper part of the Bug River watershed. In other years, TWS-GRACE data generally provide satisfactory results (correlation coefficient with high-resolution data above 0.9), and the correction mainly compensates for discrepancies due to the high temporal variance of P, which cannot be captured with the low temporal resolution of GRACE.

The correction of the TWS-GRACE series by fusion with high-resolution P, ET, R data noticeably improved the agreement between TWS-GRACE and TWS-WB. For the Bug River Basin, we obtained a root mean square error (RMSE) equal to 34.7 mm/month for non-corrected TWS-GRACE and 14.9 mm/month for TWS-GRACE after data fusion. This confirms that the combination of GRACE data with high-resolution P, ET and R data allows for a better fit to the observed components of the water balance.

TWS VARIABILITY IN THE BUG RIVER BASIN IN 2012–2023

We now focus on the temporal variability of TWS in the Bug River Basin. To do so, we analyse the TWS-GRACE time series (with and without the fusion with P, ET and R data) for various oscillations. Figure 17 shows that overall TWS variability in the Bug River Basin is primarily dominated by seasonal fluctuations and trend. Although a downward trend is observed over the entire period, the magnitude and even the direction of this trend vary when shorter time intervals are considered. For example, during the 2012–2015 period, negative TWS trends are the strongest, followed by a reversal to a positive trend in

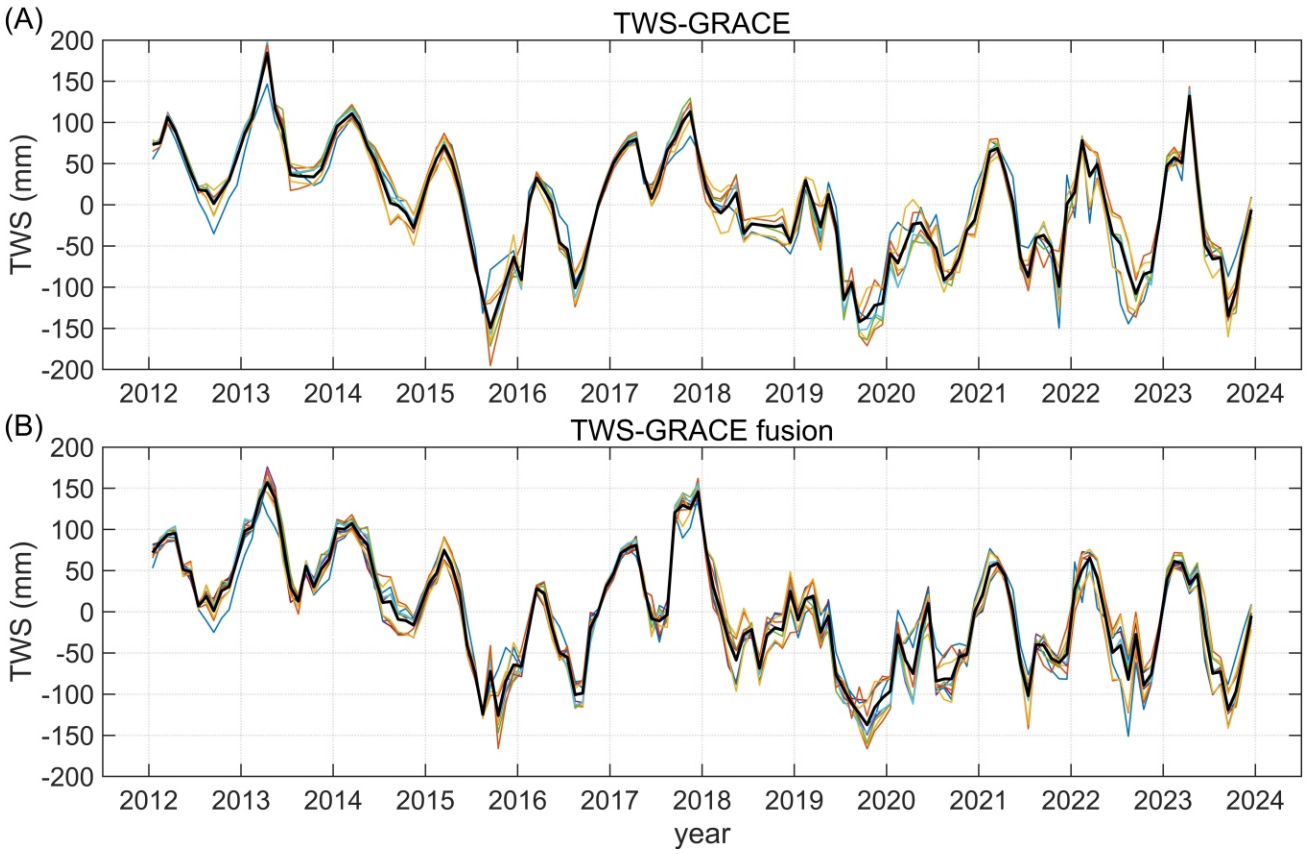

Fig. 17. Time series of TWS-GRACE for each grid computed from GRACE data (A) and from fusion of GRACE and P, ET, R data (B)

The thick black line represents the series for the average across the entire area

2016–2018, and then another intensification of negative trends in 2018–2020. Finally, from around early 2021, TWS trends are close to zero (Table 3). We also observe that during the GRACE mission period (2012–2017), the TWS-GRACE series for individual grids are almost identical, while during the GRACE-FO period (after 2018), the spatial variability of the TWS-GRACE signal increases, which is consistent with the spatial variability observed for TWS-GRACE when data fusion is applied.

To examine which periodic oscillations are typical for TWS in the region studied, we plotted the FFT amplitude spectra (Fig. 18). This figure shows that the dominant oscillation is annual (1 cycle/year) with an amplitude of ~50 mm. Another significant oscillation is the 4-year cycle (0.25 cycle/year) with an amplitude of ~40 mm. Two other oscillations with an amplitude greater than 10 mm include the 18-month (0.7 cycle/year) and 2-year (0.5 cycle/year) cycles.

Due to the dominance of the annual signal in TWS variability in the region analysed, we now focus on this oscillation, performing a detailed analysis of the amplitudes and phases of this signal, calculated using equations 6 and 7 (Fig. 19). The diagrams show that the amplitudes of annual oscillation for individual grids range from around 50 to 54 mm for TWS-GRACE without fusion and from 47 mm to 51 mm for TWS-GRACE with fusion (Table 4). Thus, data fusion results in a slight decrease in the annual oscillation amplitude by an average of 3 mm. The phase values across all grids are relatively consistent for both variants of TWS computation. However, there are some differences in phases between GRACE-TWS with and without data fusion. These discrepancies reach a maximum of 12°, which corresponds to approximately a 12-day delay in the data without fusion compared to those with data fusion. However, considering the monthly temporal resolution of the data analysed, this shift is not significant. For the area studied, the annual signal reaches its maximum value in February and its minimum value in August.

By removing the seasonal signal from the TWS series, characterized in our case by a constant amplitude and phase, we can focus on non-seasonal variations, which are crucial for identifying extreme TWS events. Figure 20 shows the time se-

Table 3

Values of linear trends (in mm/year) in TWS-GRACE for four different periods, each characterized by distinct trend patterns and for the whole period considered

	2012-01 to 2015-09	2015-09 to 2017-11	2017-11 to 2020-01	2020-01 to 2023-12	2012-01 to 2023-12
TWS-GRACE	–29.1±14.5	+91.1±19.3	–72.8±17.4	+2.7±14.9	–8.8±5.2
TWS-GRACE fusion	–26.9±13.5	+82.3±21.8	–85.2±20.5	+3.8±13.6	–8.9±5.1

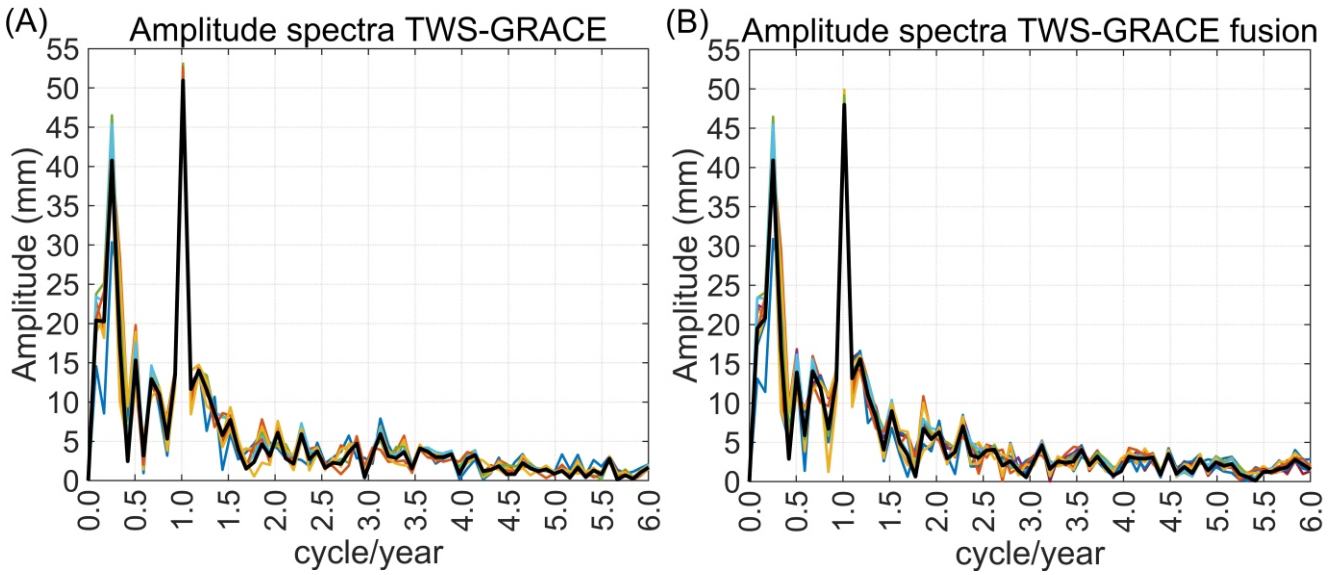

Fig. 18. FFT amplitude spectra of TWS-GRACE for each grid computed from GRACE data (A) and from fusion of GRACE and P, ET, R data (B). The thick black line represents spectra for the average across the entire area

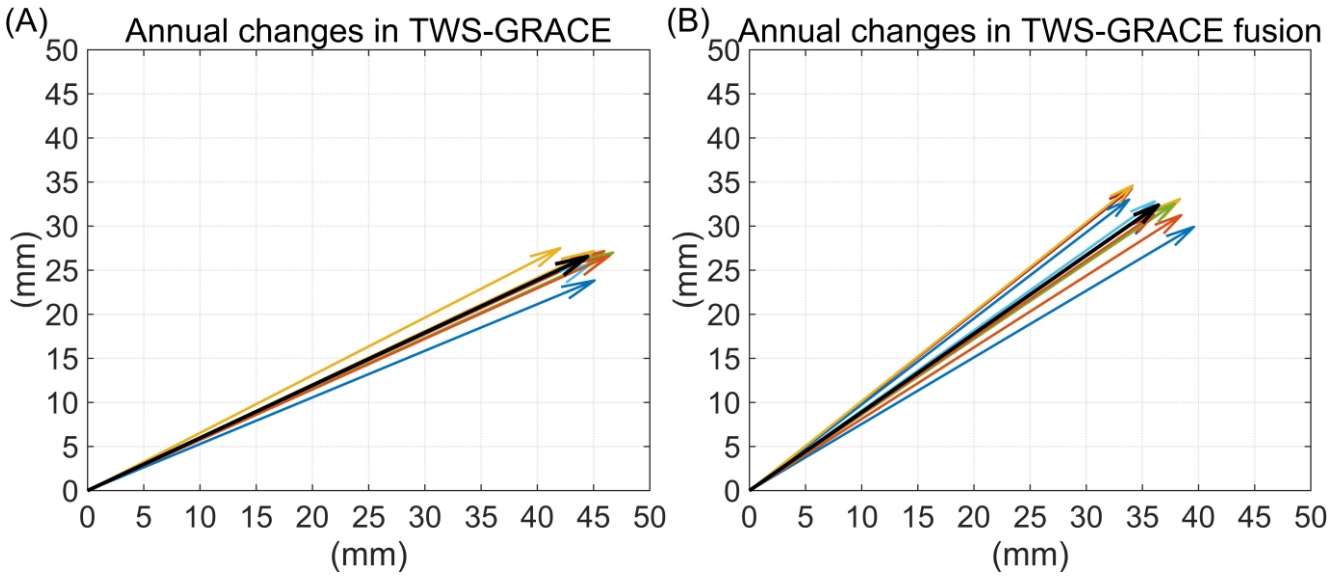

Fig. 19. Phasor diagrams of annual oscillation for TWS-GRACE for each grid computed from GRACE data (A) and from fusion of GRACE and P, ET, R data (B)

Table 4

Maximum, minimum and average values of amplitudes and phases of annual oscillation for TWS-GRACE without and with data fusion, and maximum differences between amplitudes and phases obtained from these two TWS estimates

	TWS-GRACE		TWS-GRACE fusion		Max difference	
	Amplitude (mm)	Phase (°)	Amplitude (mm)	Phase (°)	Amplitude (mm)	Phase (°)
Minimum	50.2	27.9	47.3	37.1	1.4	12.4
Maximum	54.0	33.2	50.6	45.4	5.8	8.5
Average	51.8	30.9	48.8	41.7	3.0	10.8

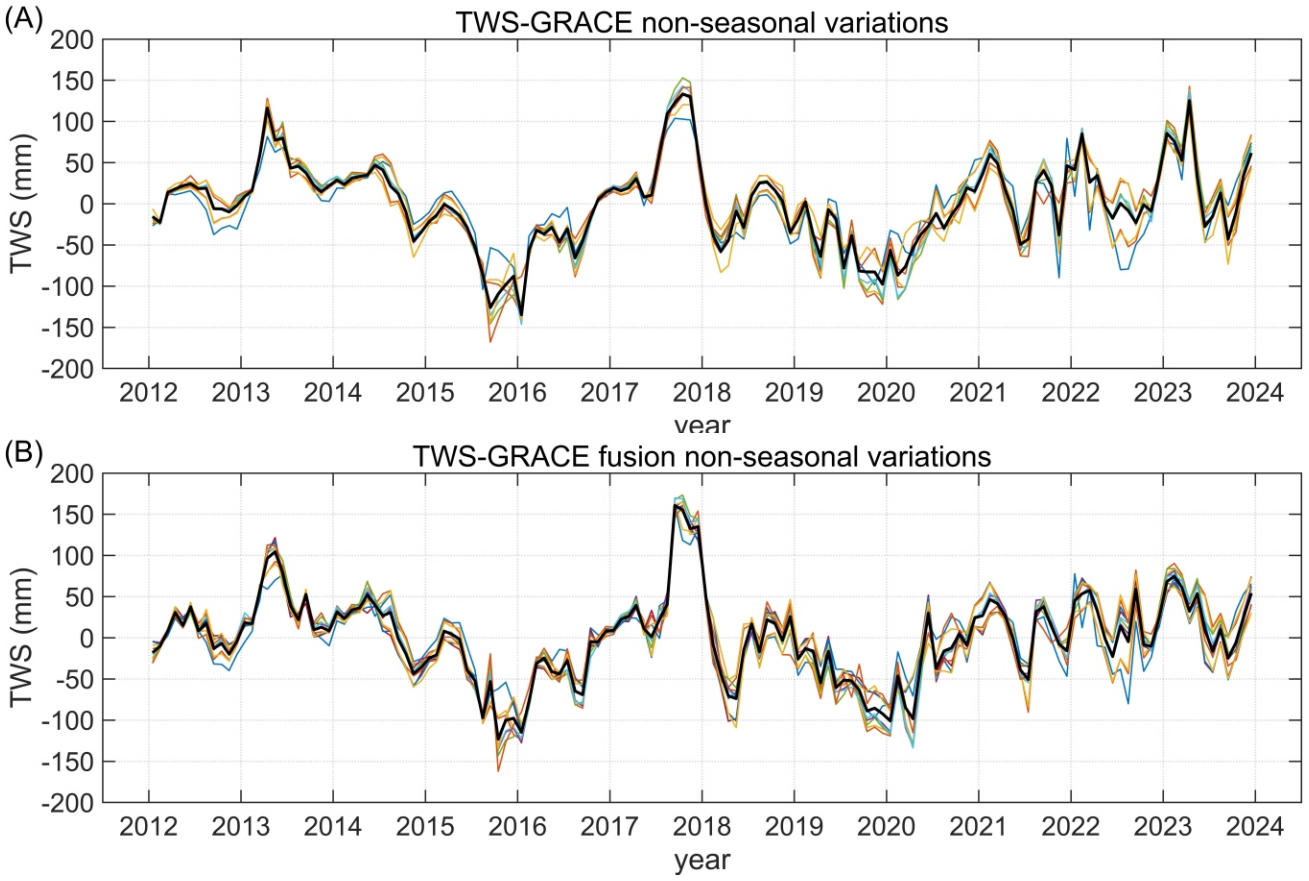

Fig. 20. Time series of non-seasonal TWS-GRACE variations for each grid computed from GRACE data (A) and from fusion of GRACE and P, ET, R data (B)

The thick black line represents the series for the average across the entire area

ries of non-seasonal TWS variations for the Bug River Basin. The figure reveals that the pattern of non-seasonal TWS changes is consistent across the entire basin. The most pronounced TWS minimum occurs in the second half of 2015, likely driven by exceptionally low precipitation in the region that year (Kundzewicz et al., 2018) and unusually high summer temperatures (Wypych et al., 2017). Another prominent minimum was recorded at the beginning of 2020. A study by Rakovec et al. (2022) emphasized that during the period 2018–2020, Europe experienced a series of exceptionally hot and dry weather conditions, which may have contributed to the observed extreme negative change in TWS. The authors identified this drought as having unprecedented intensity and duration of over two years (Rakovec et al., 2022).

In addition to the visible peaks of minima in TWS changes, maxima are also observed in the Bug River Basin region, with the first occurring in May-June 2013 and the second, stronger one in the second half of 2017. The maxima largely reflect above-normal precipitation levels in the region, which in extreme cases led to flooding. This was the case in 2013 when flooding affected many countries in Central Europe (Merz et al., 2014). Although the flood primarily impacted Germany, the Czech Republic and Austria, intense rainfall was also observed in Poland during this period. Meteorological observations showed that also in 2017 precipitation totals exceeded the long-term average in the majority of months (IMGW, 2021). An analysis of non-seasonal TWS changes shows that between 2012 and 2021, alternating anomalous minima and maxima in TWS were observed in the region, occurring approximately every two years (i.e., an exceptional increase in TWS every four years, followed by an exceptional decrease in TWS every four years). However, it is apparent that over the past four years, a change has occurred in this pattern, and the observed peaks of minima and maxima are no longer as pronounced, which is reflected in the disappearance of the 4-year oscillation in the plot of long-term non-seasonal TWS variations (Fig. 21).

In the era of climate change, there is a need to prepare for more frequent and intense extreme weather events, such as floods and droughts, which have recently occurred in quick succession (for example, in Poland in 2024, where a dry summer was followed by heavy autumn rains, causing floods in the southern part of the country). Climate projections indicate that the Bug River Basin region will experience a notable warming trend throughout the 21st century. The SSP1 scenario, which assumes sustainable development, projects that the mean annual temperature will rise by 2°C by the mid-21st century and then stabilize. However, the SSP5 scenario, which appears to be more realistic, suggests a more drastic temperature increase, potentially reaching a 6°C rise by the end of the century (Snizhko et al., 2024b). At the same time, the work by Rakovec et al. (2022) noted that future drought events in Europe could reach a comparable intensity to the exceptional 2018–2020 drought, but with significantly longer durations.

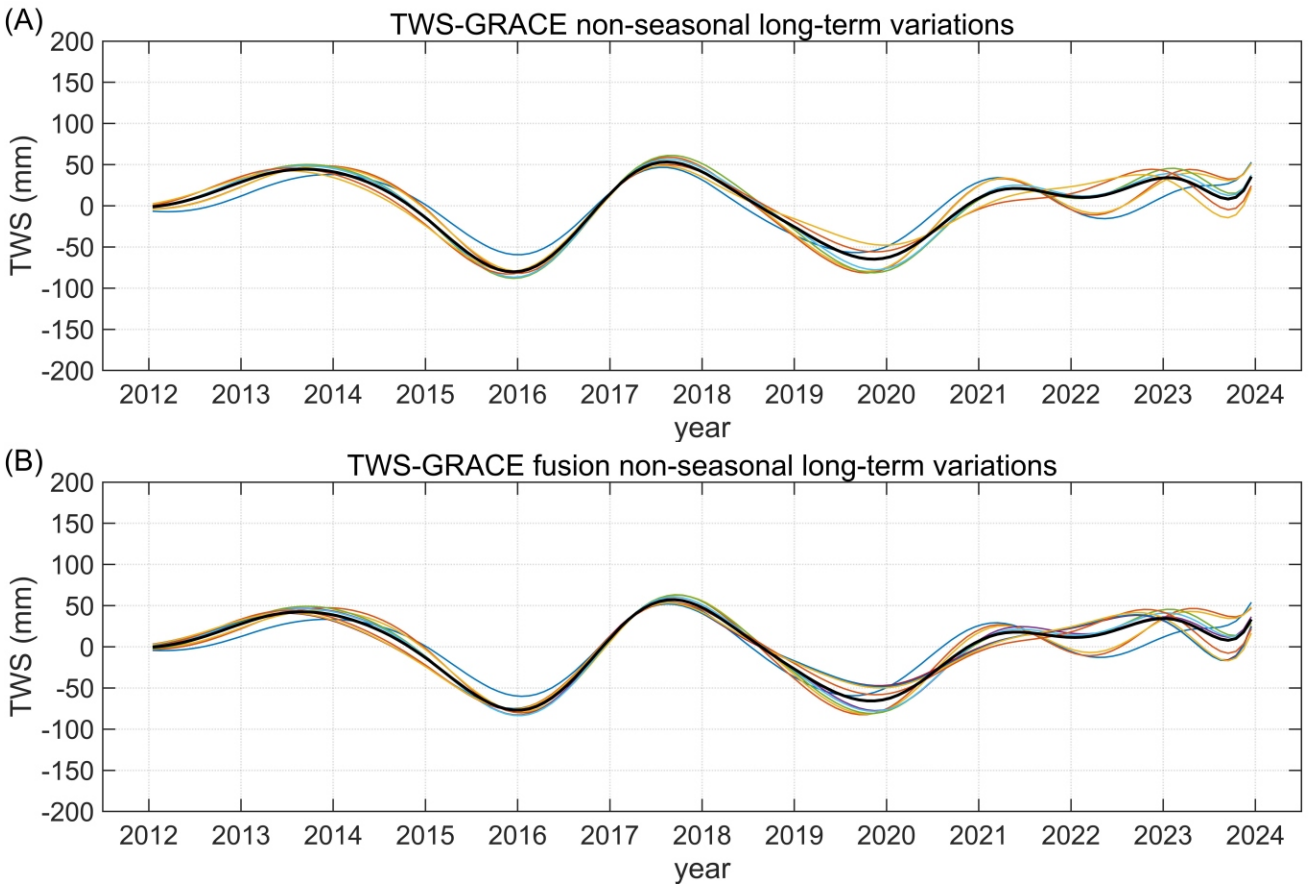

Fig. 21. Time series of non-seasonal long-term TWS-GRACE variations for each grid computed from GRACE data (A) and from fusion of GRACE and P, ET, R data (B)

The thick black line represents the series for the average across the entire area

DISCUSSION

GRACE data have relatively low spatial resolution, and this also applies to mascon solutions, which differ from solutions based on the classical approach utilizing SH coefficients in that they do not require filtering, thus avoiding the risk of losing part of the actual signal. Although mascon data are generally more reliable for regional analyses, they do not contain any additional geophysical information at higher resolution compared to SH data.

Therefore, we developed a statistical model for the fusion of TWS-GRACE with higher-resolution P, ET and R data (Loomis et al., 2019). The model assumes that the value of TWS results from the proportion between the positive (P) and negative (ET and R) components of the water balance, and serves as a compensatory component (determined by the imbalance in the water balance). The water balance approach is widely used, transparent, and its effectiveness in analysing TWS and its driving factors has been proven (Sahoo et al., 2011; Getirana et al., 2014; Long et al., 2015). However, any inaccuracies in the P, ET, and R data will accumulate in the water balance closure and thus distort the actual TWS value (Li et al., 2023). Therefore, our model was designed so that the simulated TWS is the result of the correction of TWS-GRACE only in part, referred to as the "residual," based on a Least Squares Regression model between the GRACE data and the water balance closure.

The reliability of simulations in the deterministic model applied is largely dependent on the accuracy of P, ET and R. Precipitation, which is the most important input variable, comes from the E-OBS database, which is based on in-situ station data. This dataset is characterized by high quality in the target area (Cornes et al., 2018). Another significant determinant is ET, which in the study area reaches values almost equal to P in the water balance. Numerous publications indicated that ET is associated with the greatest uncertainty (15–30%), also due to the sparse network of *in situ* stations (Rodell et al., 2004; Sahoo et al., 2011; Li et al., 2023). In light of the above considerations, the water balance estimation of TWS is associated with uncertainty. However, compared to the interpolation of raw GRACE data, it provides better results for improving the spatial resolution of GRACE, as it relies on physical data.

The lack of an *in situ* TWS measurement equivalent makes validating the GRACE signal a challenge. Because of this, TWS-GRACE corrected by fusion with high-resolution P, ET and R data was compared with TWS estimated from the water balance approach. After the fusion of GRACE data with P, ET and R data, a noticeable improvement in agreement with TWS obtained from the water balance approach was achieved (RMSE reduction from 34.7 to 14.9 mm/month). This is the first attempt to increase the resolution of TWS-GRACE using measurement data of water balance components. With this approach, we demonstrate that TWS changes occur not only at the basin scale but also in individual grid cells of the measurement grid (Solovey et al., 2024).

The results obtained, as predicted, show that TWS variability is dominated by precipitation, particularly in the upper part of

the Bug Basin. Therefore, in most cases, the correction of TWS-GRACE involved compensating for the large temporal variability of precipitation, which is not detectable to the same extent by GRACE. The greatest benefits from the fusion of GRACE data with P, ET and R data were achieved in years with poor GRACE data quality (2020) or a lack of GRACE measurements (2017, 2018). During these periods, the correlation between TWS-GRACE and TWS-WB was increased from 0.13–0.35 to 0.99 after fusion with P, ET and R.

The impact of data fusion in TWS-GRACE is most evident in the correction of extreme values. Maximum values generally required reduction, while minimum values required an increase (Table 2). Additionally, the developed model compensated for the overestimation of the downward trend in TWS-GRACE. Water balance observations indicate that in the dry season (April-September), with ET exceeding P, the downward trend in TWS is somewhat smaller, while in the wet season (October-March), it is larger. Importantly, TWS-GRACE data show a greater intensity of water resource depletion than the water balance calculations. It cannot be ruled out that groundwater exploitation contributes to this effect to some extent. This issue requires further clarification in the future, based on groundwater monitoring data.

CONCLUSIONS

Central and Southern Europe is experiencing drying due to increased ET and air temperature, despite stable precipitation levels. In the Bug River Basin, TWS decreased at a rate of 8.8±5.2 mm/year from 2012 to 2023, according to GRACE observations. To validate this trend, we conducted an analysis of the spatial and temporal mismatch patterns between TWS-GRACE and estimates derived from the water budget. We applied ensemble data assimilation techniques to integrate hydrometeorological data and TWS-GRACE. The regression models obtained for simulating TWS were used to correct TWS-GRACE. The results of the calculations show that TWS fusion effectively compensates for the uncertainties in TWS-GRACE related to low spatial and temporal resolution. The correlation analysis between TWS with data fusion and TWS-GRACE allowed for the detection of errors in GRACE solutions and popular autoregressive methods for filling gaps in GRACE measurements. The results demonstrate that the developed model significantly improved the agreement between TWS-GRACE and TWS-WB (according to RMSE, from 34.7 to 14.9 mm/month).

Our data fusion method which is based on combining GRACE data with P, ET and R, provides an alternative to extrapolating TWS-GRACE time series beyond the GRACE measurement period. The results of our research may also prove useful for downscaling GRACE data, as well as for spatial and temporal interpolation, which has long been a challenge in water resources studies.

One of the key limitations of satellite gravimetry in assessing regional TWS variations is its relatively coarse spatial resolution, which restricts its applicability in small catchments, especially those with heterogeneous topography or complex hydrological systems. As such, a logical next step is to pursue the downscaling of TWS-GRACE data using advanced algorithms, supported by high-resolution model outputs and in situ observations.

Another important direction for future research is the monitoring of changes in groundwater storage, which, in our study area, accounts for up to 70% of drinking water supply. Integrating downscaled GRACE-derived data with high-resolution information on water balance components can enhance the monitoring of these crucial resources, especially in regions where the ground-based monitoring network is sparse or unevenly distributed. Moreover, the application of advanced techniques, including machine learning methods, offers the potential not only to enhance the understanding of groundwater dynamics but also to enable more accurate forecasting, which is crucial for the sustainable management of groundwater resources.

Acknowledgements. This research was funded by the National Science Centre, Poland, under the IMPRESS-U call (grant number 2023/05/Y/ST10/00234) and co-financed from national funds (grant number 61.8109.2500.00.0). We also thank the Associate Editor and two reviewers for their constructive comments that improved this manuscript.

Data Availability Statement. GRACE/GRACE-FO CSR RL06.3 solution was provided by the Center for Space Research and accessed from the following website: https://www2.csr.utexas.edu/grace/RL06_mascons.html. Precipitation data from E-OBS are available at: https://data.usgs.gov/modelcatalog/model/442e41e9-6039-4224-9722-64b648c9defa. Evapotranspiration data from SSEBop were obtained from the website https://earlywarning.usgs.gov/fews/product/460. River discharge data was retrieved from the collections of the Institute of Meteorology and Water Management in Poland and the Institute of Hydrometeorology of Ukraine (https://danepubliczne.imgw.pl/datastore).

REFERENCES

Becker, M., Meyssignac, B., Xavier, L., Cazenave, A., Alkama, R., Decharme, B., 2011. Past terrestrial water storage (1980–2008) in the Amazon Basin reconstructed from GRACE and in situ river gauging data. Hydrology and Earth System Sciences, **15**: 533–546; https://doi.org/10.5194/hess-15-533-2011

Box, G.E.P., Jenkins, G.M., Reinsel, G.C., Ljung, G.M., 2016. Time Series Analysis: Forecasting and Control, 5th ed., John Wiley and Sons Inc., Hoboken, N. J., USA.

Brigham, E.O., Morrow, R.E., 1967. The Fast Fourier Transform. IEEE Spectrum, **4**: 63–70; https://doi.org/10.1109/MSPEC.1967.5217220

Butterworth, S., 1930. On the theory of filter amplifiers. Experimental Wireless and the Wireless Engineer, **7**: 536–541.

Chen, J., Cazenave, A., Dahle, C., Lovel, W., Panet, I., Pfeffer, J., Moreira, L., 2022. Applications and challenges of GRACE and GRACE follow-on satellite gravimetry. Surveys in Geophysics, **43**: 305–345; https://doi.org/10.1007/s10712-021-09685-x

Cornes, R.C., van der Schrier, G., van den Besselaar, E.J.M., Jones, P.D., 2018. An ensemble version of the E-OBS temperature and precipitation datasets. Journal of Geophysical Research: Atmospheres, **123**: 9391–9409; https://doi.org/10.1029/2017JD028200

Duveiller, G., Donatelli, M., Fumagalli, D., Zucchini, A., Nelson, R., Baruth, B., 2017. A dataset of future daily weather data for crop modelling over Europe derived from climate change scenarios. Theoretical and Appliead Climatology, **127**: 573–585; https://doi.org/10.1007/s00704-015-1650-4

Fibbi, L., Chiesi, M., Moriondo, M., Bindi, M., Chirici, G., Papale, D., Gozzini, B., Maselli, F., 2016. Correction of a 1 km daily rainfall dataset for modelling forest ecosystem processes in Italy. Meteorological Application, **23**: 294–303; https://doi.org/10.1002/met.1554

Forootan, E., Schumacher, M., Mehrnegar, N., Bezděk, A., Talpe, M.J., Farzaneh, S., Zhang, C., Zhang, Y., Shum, C.K., 2020. An iterative ICA-based reconstruction method to produce consistent time-variable total water storage fields using GRACE and swarm satellite data. Remote Sensing, **12**, 1639; https://doi.org/10.3390/rs12101639

Frappart, F., Seoane, L., Ramillien, G., 2013. Validation of GRACE-derived terrestrial water storage from a regional approach over South America. Remote Sensing of Environment, **137**: 69–83; https://doi.org/10.1016/j.rse.2013.06.008

Frappart, F., Ramillien, G., 2018. Monitoring groundwater storage changes using the gravity recovery and climate experiment (GRACE) satellite mission: a review. Remote Sensing, **10**, 829; https://doi.org/10.3390/rs10060829

Getirana, A., Dutra, E., Guimberteau, M., Kam, J., Li, H., Decharme, B., Sheffield, J., 2014. Water balance in the Amazon basin from a land surface model ensemble. Journal of Hydrometeorology, **15**: 2586–2614; https://doi.org/10.1175/JHM-D-14-0068.1

Gopchak, I., Kalko, A., Basiuk, T., Pinchuk, O., Gerasimov, I., Yaromenko, O., Shkirynets, V., 2020. Assessment of surface water pollution in western Bug River within the cross-border section of Ukraine. Journal of Water and Land Development, **46** (VII–IX): 97–104; https://doi.org/10.24425/jwld.2020.134201

Grzywna, A., Bronowicka-Mielniczuk, U., Połeć, K., 2021. Spatio-temporal changes of water pollution, and its sources and consequences in the Bug River, Poland. Desalination and Water Treatment, **243**: 18–36; https://doi.org/10.5004/dwt.2021.27848

Gyawali, B., Ahmed, M., Murgulet, D., Wiese, D.N., 2022. Filling temporal gaps within and between GRACE and GRACE-FO terrestrial water storage records: an innovative approach. Remote Sensing, **14**, 1565; https://doi.org/10.3390/rs14071565

Hassan, A., Jin, S., 2016. Water storage changes and balances in Africa observed by GRACE and hydrologic models. Geodesy and Geodynamics, **7**: 39–49; https://doi.org/10.1016/j.geog.2016.03.002.

Haylock, M.R., Hofstra, N., Klein Tank, A.M.G., Klok, E.J., Jones, P.D., New, M., 2008. A European daily high-resolution gridded data set of surface temperature and precipitation for 1950–2006. Journal of Geophysical Research, **114**, D20119; https://doi.org/10.1029/2009JD011799

Hu, B., Wang, L., Li, X., Zhou, J., Pan, Y., 2021. Divergent changes in terrestrial water storage across global arid and humid basins. Geophysical Research Letters, **48**, e2020GL091069; https://doi.org/10.1029/2020GL091069

IMGW, 2021. Climate of Poland 2020. Accessed 3 November 2024, https://www.imgw.pl/sites/default/files/2021-04/imgw-pib-klimat-polski-2020-opracowanie-final-eng-pojedyncze-min.pdf

Jing, W., Zhang, P., Zhao, X., 2019. A comparison of different GRACE solutions in terrestrial water storage trend estimation over Tibetan Plateau. Scientific Reports, **9**, 1765; https://doi.org/10.1038/s41598-018-38337-1

Klok, E.J., Klein Tank, A.M.G., 2008. Updated and extended European dataset of daily climate observations. International Journal of Climatology, **29**: 1182–1191; https://doi.org/10.1002/joc.1779

Kondracki, J., 2011. Geografia regionalna Polski (in Polish). Wyd. Naukowe PWN, Warszawa.

Kostrzewski, A., Abramowicz, D., 2023. Geoprzestrzeń 7. Kompleksowe badania środowiska geograficznego (in Polish). Bogucki Wyd. Naukowe, Poznań.

Kundzewicz, Z.W., Piniewski, M., Mezghani, A., Okruszko, T., Pinskwar, I., Kardel, I., Øystein, H., Szczęśniak, M., Szwed, M., Benestad, R., Marcinkowski, P., Graczyk, D., Dobler, A., Førland, E.J., O'Keefe, J., Choryński, A., Parding, K.M., Haugen, J.E., 2018. Assessment of climate change and associated impact on selected sectors in Poland. Acta Geophysica, **66**: 1509–1523; https://doi.org/10.1007/s11600-018-0220-4

Landerer, F.W., Flechtner, F.M., Save, H., Webb, F.H., Bandikova, T., Bertiger, W.I., et al., 2020. Extending the global mass change data record: GRACE Follow-On instrument and science data performance. Geophysical Research Letters, **47**, e2020GL088306; https://doi.org/10.1029/2020GL088306

Lavaysse, C., Camalleri, C., Dosio, A., van der Schrier, G., Toreti, A., Vogt, J., 2017. Towards a monitoring system of temperature extremes in Europe. Natural Hazards and Earth System Sciences Discuss, **18**: 91–104; https://doi.org/10.5194/nhess-2017-181

Li, C., Yu, Q., Zhang, Y., Ma, N., Tian, J., Zhang, X., 2023. Dominant drivers for terrestrial water storage changes are different in northern and southern China. Journal of Geophysical Research: Atmospheres, **128**, e2022JD038074; https://doi.org/10.1029/2022JD038074

Li, F., Kusche, J., Rietbroek, R., Wang, Z., Forootan, E., Schulze, K., Lück, C., 2020. Comparison of data-driven techniques to reconstruct (1992–2002) and predict (2017–2018) GRACE-like gridded total water storage changes using climate inputs. Water Resources Research, **56**, e2019WR026551; https://doi.org/10.1029/2019WR026551

Long, D., Yang, Y., Wada, Y., Hong, Y., Liang, W., Chen, Y., Yong, B., Hou, A., Wei, J., Chen, L., 2015. Deriving scaling factors using a global hydrological model to restore GRACE total water storage changes for China's Yangtze River Basin. Remote Sensing of Environment, **168**: 177–193; https://doi.org/10.1016/j.rse.2015.07.003

Longuevergne, L., Scanlon, B.R., Wilson, C.R., 2010. GRACE Hydrological estimates for small basins: Evaluating processing approaches on the High Plains Aquifer, USA. Water Resources Research, **46**, W11517; https://doi.org/10.1029/2009WR008564

Loomis, B.D., Luthcke, S.B., Sabaka, T.J., 2019. Regularization and error characterization of GRACE mascons. Journal of Geodesy, **93**: 1381–1398; https://doi.org/10.1007/s00190-019-01252-y

Lorenc, H. (ed.), 2005. Atlas klimatu Polski (in Polish). Instytut Meteorologii i Gospodarki Wodnej, Warszawa.

Lorenz, C., Devaraju, B., Tourian, M.J., Sneeuw, N., Riegger, J., Kunstmann, H., 2014. Large-scale runoff from landmasses: A global assessment of the closure of the hydrological and atmospheric water balances. Journal Hydrometeorology, **15**: 2111–2139; https://doi.org/10.1175/JHM-D-13-0157.1

Merz, B., Elmer, F., Kunz, M., Mühr, B., Schröter, K., Uhlemann-Elmer, S., 2014. The extreme flood in June 2013 in Germany. La Houille Blanche, **100**: 5–10; https://doi.org/10.1051/lhb/2014001

Min, E., Hazeleger, W., van Oldenborgh, G.J., Sterl, A., 2013. Evaluation of trends in high temperature extremes in North-Western Europe in regional climate models. Environmental Research Letters, **8**, 14011; https://doi.org/10.1088/1748-9326/8/1/014011

Miro, M.E., Famiglietti, J.S., 2018. Downscaling GRACE Remote sensing datasets to high-resolution groundwater storage change maps of California's Central Valley. Remote Sensing, **10**, 143; https://doi.org/10.3390/rs10010143

Nanteza, J., de Linage, C.R., Thomas, B.F., Famiglietti, J.S., 2016. Monitoring groundwater storage changes in complex basement aquifers: an evaluation of the GRACE satellites over East Africa. Water Resources Research, **52**: 9542–9564; https://doi.org/10.1002/2016WR018846

Nikulin, G., Kjellstrom, E., Hansson, U.L.F., Strandberg, G., Ullerstig, A., 2011. Evaluation and future projections of temperature, precipitation and wind extremes over Europe in an ensemble of regional climate simulations. Tellus A: Dynamic Meteorology and Oceanography, **63**: 41–55; https://doi.org/10.1111/j.1600-0870.2010.00466.x

Pascal, C., Ferrant, S., Selles, A., Maréchal, J.-C., Paswan, A., Merlin, O., 2022. Evaluating downscaling methods of GRACE (Gravity Recovery and Climate Experiment) data: a case study over a fractured crystalline aquifer in southern India. Hydrology and Earth System Sciences, **26**: 4169–4186; https://doi.org/10.5194/hess-26-4169-2022

Preisendorfer, R.W., 1988. Principal Component Analysis in Meteorology and Oceanography. Elsevier, Amsterdam.

Rakovec, O., Samaniego, L., Hari, V., Markonis, Y., Moravec, V., Thober, S., Hanel, M., Kumar, R., 2022. The 2018–2020 multi-year drought sets a new benchmark in Europe. Earth's Future, **10**, e2021EF002394; https://doi.org/10.1029/2021EF002394

Ran, J., Ditmar, P., Klees, R., 2018. Optimal mascon geometry in estimating mass anomalies within Greenland from GRACE. Geophysical Journal International, **214**: 2133–2150; https://doi.org/10.1093/gji/ggy242

Rodell, M., Famiglietti, J.S., Chen, J., Seneviratne, S.I., Viterbo, P., Holl, S., Wilson, C.R., 2004. Basin scale estimates of evapotranspiration using GRACE and other observations. Geophysical Research Letters, **31**, L20504; https://doi.org/10.1029/2004GL020873

Rowlands, D.D., Luthcke, S.B., Klosko, S.M., Lemoine, F.G.R., Chinn, D.S., McCarthy, J.J., Cox, C.M., Anderson, O.B., 2005. Resolving mass flux at high spatial and temporal resolution using GRACE intersatellite measurements. Geophysical Research Letters, **32**, L04310; https://doi.org/10.1029/2004GL021908

Sahoo, A., Pan, M., Troy, T.J., Vinukollu, R.K., Sheffield, J., Wood, E.F., 2011. Reconciling the global terrestrial water budget using satellite remote sensing. Remote Sensing of Environment, **115**: 1850–1865; https://doi.org/10.1016/j.rse.2011.03.009

Save, H., 2020. CSR GRACE and GRACE-FO RL06 Mascon Solutions v02. Accessed 14 October 2024; https://doi.org/10.15781/cgq9-nh24

Save, H., Bettadpur, S., Tapley, B.D., 2016. High resolution CSR GRACE RL05 mascons. Journal of Geophysical Research: Solid Earth, **121**: 7547–7569; https://doi.org/10.1002/2016JB013007

Savoca, M.E., Senay, G.B., Maupin, M.A., Kenny, J.F., Perry, C.A., 2013. Actual evapotranspiration modeling using the operational Simplified Surface Energy Balance (SSEBop) approach. Scientific Investigations Report 2013–5126. Groundwater Resources Program. U.S. Geological Survey; https://doi.org/10.3133/sir20135126

Scanlon, B.R., Zhang, Z., Save, H., Wiese, D.N., Landerer, F.W., Long, D., Longuevergne, L., Chen, J., 2016. Global evaluation of new GRACE mascon products for hydrologic applications. Water Resources Research, **52**: 9412–9429; https://doi.org/10.1002/2016WR019494

Senay, G.B., 2018. Satellite psychrometric formulation of the Operational Simplified Surface Energy Balance (SSEBop) model for quantifying and mapping evapotranspiration. Applied Engineering in Agriculture, **34**: 555–566; https://doi.org/10.13031/aea.12614

Shakhman, I., Bystriantseva, A., 2020. Water quality assessment of the surface water of the southern Bug River Basin by complex indices. Journal of Ecological Engineering, **22**: 195–205; https://doi.org/10.12911/22998993/128858

Snizhko, S., Didovets, I., Bronstert, A., 2024a. Ukraine's water security under pressure: climate change and wartime. Water Security, **23**, 100182; https://doi.org/10.1016/j.wasec.2024.100182

Snizhko, S., Didovets, I., Shevchenko, O., Yatsiuk, M., Hattermann, F.F., Bronstert, A., 2024b. Southern Bug River: water security and climate changes perspectives for post-war city of Mykolaiv, Ukraine. Frontiers in Water, **6**, 1447378; https://doi.org/10.3389/frwa.2024.1447378

Solovey, T., Śliwińska-Bronowicz, J., Janica, R., Brzezińska, A., 2024. High-resolution groundwater storage changes from GRACE/GRACE-FO using assimilation models and hydrogeological observations. „globalwaterstorage.info", Helmholtz Centre Potsdam; https://www.globalwaterstorage.info/en/high-resolution-groundwater-storage-changes-from-grace/grace-fo-using-assimilation-models-and-hydrogeological-observations

Somorowska, U., 2021. Czasowa zmienność i przestrzenne zróżnicowanie ewapotranspiracji w zlewni nizinnej rzeki Łasicy (in Polish). Prace i Studia Geograficzne, **66**: 35–46; https://doi.org/10.48128/pisg/2021-66.3-03

Sun, A.Y., Scanlon, B.R., Zhang, Z., Walling, D., Bhanja, S.N., Mukherjee, A., Zhong, Z., 2019. Combining physically based modeling and deep learning for fusing GRACE satellite data: Can we learn from mismatch? Water Resources Research, **55**: 1179–1195; https://doi.org/10.1029/2018WR023333

Sun, A.Y., Scanlon, B.R., Save, H., Rateb, A., 2021. Reconstruction of GRACE total water storage through automated machine learning. Water Resources Research, **57**, e2020WR028666; https://doi.org/10.1029/2020WR028666

Szwed, M., 2015. The Elements of Water Balance in the Changing Climate in Poland. Advances in Meteorology, **2015**, 149674; https://doi.org/10.1155/2015/149674

Tapley, B.D., Bettadpur, S., Watkins, M., Reigber, C., 2004. The gravity recovery and climate experiment: Mission overview and early results. Geophysical Research Letters, **31**, L09607; https://doi.org/10.1029/2004GL019920

Tapley, B.D., Watkins, M.M., Flechtner, F. et al., 2019. Contributions of GRACE to understanding climate change. Nature Climate Change, **9**: 358–369; https://doi.org/10.1038/s41558-019-0456-2

Tourian, M.J., Reager, J.T., Sneeuw, N., 2018. The total drainable water storage of the Amazon river basin: a first estimate using GRACE. Water Resources Research, **54**: 3290–3312; https://doi.org/10.1029/2017WR021674

Urban, G., Kuchar, L., Kempińska-Kasprzak, M., Łaszyca, E., 2022. A Climatic water balance variability during the growing season in Poland in the context of modern climate change. Meteorologische Zeitschrift, **31**: 349–365; https://doi.org/10.1127/metz/2022/1128

van der Linden P., Mitchell, J.F.B. (eds.), 2009. ENSEMBLES: Climate Change and its Impacts: Summary of research and results from the ENSEMBLES project. Met Office Hadley Centre, FitzRoy Road, Exeter EX1 3PB, UK. 160 pp. Accessed 13 March 2024; https://ensembles-eu.metoffice.gov.uk/docs/Ensembles_final_report_Nov09.pdf

van Dijk, A.I.J.M., Renzullo, L.J., Wada, Y., Tregoning, P., 2014. A global water cycle reanalysis (2003–2012) merging satellite gravimetry and altimetry observations with a hydrological multi-model ensemble. Hydrology and Earth System Sciences, **18**: 2955–2973; https://doi.org/10.5194/hess-18-2955-2014

van Oldenborgh, G.J., Philip, S., Aalbers, E., Vautard, R., Otto, F., Haustein, K., Habets, F., Singh, R., Cullen, H., 2016. Rapid attribution of the May/June 2016 flood-inducing precipitation in France and Germany to climate change. Hydrology and Earth System Sciences; https://doi.org/10.5194/hess-2016-308

Velicogna, I., Mohajerani, Y., Landerer, F., Mouginot, J., Noel, B., Rignot, E., Sutterley, T., van den Broeke, M., van Wessem, M., Wiese, D., 2020. Continuity of ice sheet mass loss in Greenland and Antarctica from the GRACE and GRACE Follow-On missions. Geophysical Research Letters, **47**, e2020GL087291; https://doi.org/10.1029/2020GL087291

Vishwakarma, B.D., Devaraju, B., Sneeuw, N., 2016. Minimizing the effects of filtering on catchment scale GRACE solutions. Water Resources Research, **52**: 5868–5890; https://doi.org/10.1002/2016WR018960

Vishwakarma, B.D., Devaraju, B., Sneeuw, N., 2018. What is the spatial resolution of GRACE satellite products for hydrology? Remote Sensing, **10**, 852; https://doi.org/10.3390/rs10060852

Vishwakarma, B.D., Zhang, J., Sneeuw, N., 2021. Downscaling GRACE total water storage change using partial least squares regression. Scientific Data, **8**, 95; https://doi.org/10.1038/s41597-021-00862-6

Wahr, J., Swenson, S., Zlotnicki, V., Velicogna, I., 2004. Time-variable gravity from GRACE: First results. Geophysical Research Letters, **31**, L11501; https://doi.org/10.1029/2004GL019779

Wahr, J., Swenson, S., Velicogna, I., 2006. Accuracy of GRACE mass estimates. Geophysical Research Letters, **33**: 1–5; https://doi.org/10.1029/2005GL025305

Watkins, M.M., Wiese, D.N., Yuan, D.N., Boening, C., Landerer, F.W., 2015. Improved methods for observing Earth's time variable mass distribution with GRACE using spherical cap mascons. Journal of Geophysical Research: Solid Earth, **120**: 2648–2671; https://doi.org/10.1002/2014JB011547

Wrzesiński, L., Sobkowiak, L., 2018. Detection of changes in flow regime of rivers in Poland, Journal of Hydrology and Hydromechanics, **66**: 55–64; https://doi.org/10.1515/johh-2017-0045

Wypych, A., Sulikowska, A., Ustrnul, Z., Czekierda, D., 2017. Temporal variability of summer temperature extremes in Poland. Atmosphere, **8**, 51; https://doi.org/10.3390/atmos8030051

Yin, W., Zhang, G., Liu, F., Zhang, D., Zhang, X., Chen, S., 2022. Improving the spatial resolution of GRACE-based groundwater storage estimates using a machine learning algorithm and hydrological model. Hydrogeological Journal, **30**: 947–963; https://doi.org/10.1007/s10040-021-02447-4

Zhong, D., Wang, S., Li, J., 2021. A self-calibration variance-component model for spatial downscaling of GRACE observations using land surface model outputs. Water Resources Research, **57**, e2020WR028944; https://doi.org/10.1029/2020WR028944